AD-A114 468 NAVAL POSTGRADUATE SCHOOL MONTEREY CA F/G 7/4
AN ELECTROCHEMICAL INVESTIGATION OF CORROSION RATES FOR 1020 ST--ETC(U)
JUN 81 D R SCOTT

UNCLASSIFIED NL

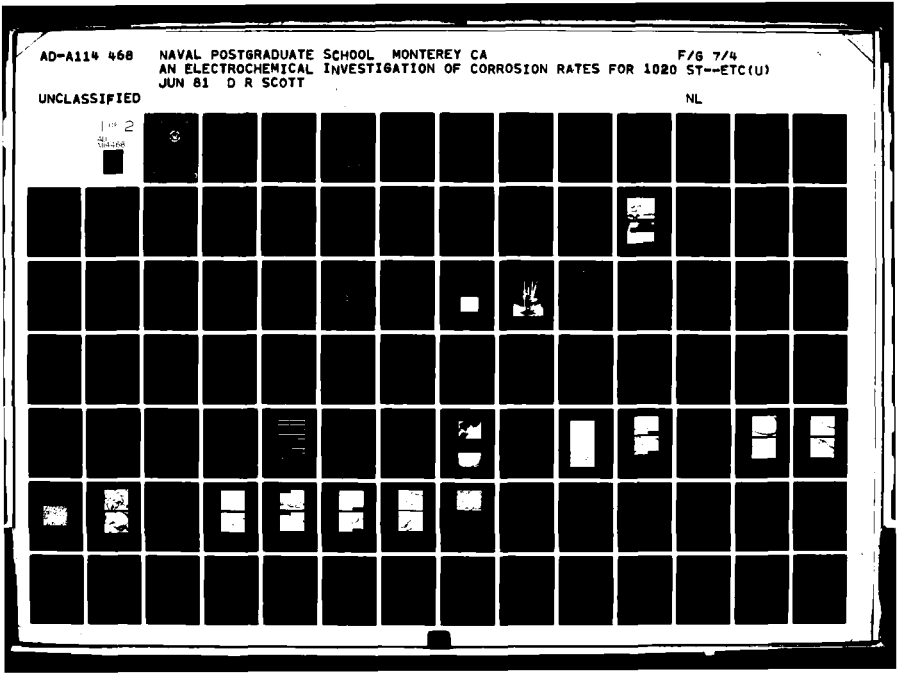

NAVAL POSTGRADUATE SCHOOL
Monterey, California

THESIS

An Electrochemical Investigation Of Corrosion Rates For 1020 Steel In Environments Which Simulate Conditions In Marine Reinforced Concrete

by

Dale Randolph Scott

June 1981

Thesis Advisor: Jeff Perkins

Approved for public release; distribution unlimited

Unclassified

SECURITY CLASSIFICATION OF THIS PAGE (When Data Entered)

REPORT DOCUMENTATION PAGE	READ INSTRUCTIONS BEFORE COMPLETING FORM
1. REPORT NUMBER	2. GOVT ACCESSION NO. AD-A124468	3. RECIPIENT'S CATALOG NUMBER
4. TITLE (and Subtitle) An Electrochemical Investigation of Corrosion Rates for 1020 Steel in Environments Which Simulate Conditions in Marine Reinforced Concrete	5. TYPE OF REPORT & PERIOD COVERED Master's Thesis June 1981
	6. PERFORMING ORG. REPORT NUMBER
7. AUTHOR(s) Dale Randolph Scott	8. CONTRACT OR GRANT NUMBER(s)
9. PERFORMING ORGANIZATION NAME AND ADDRESS Naval Postgraduate School Monterey, California	10. PROGRAM ELEMENT, PROJECT, TASK AREA & WORK UNIT NUMBERS
11. CONTROLLING OFFICE NAME AND ADDRESS Naval Postgraduate School Monterey, California	12. REPORT DATE June 1981
	13. NUMBER OF PAGES 111
14. MONITORING AGENCY NAME & ADDRESS(if different from Controlling Office)	15. SECURITY CLASS. (of this report)
	15a. DECLASSIFICATION/DOWNGRADING SCHEDULE

16. DISTRIBUTION STATEMENT (of this Report)

Approved for public release; distribution unlimited.

17. DISTRIBUTION STATEMENT (of the abstract entered in Block 20, if different from Report)

18. SUPPLEMENTARY NOTES

19. KEY WORDS (Continue on reverse side if necessary and identify by block number)

Reinforced Concrete
Electrochemical Investigation
Saturated $Ca(OH)_2$
Chlorides
Dissolved Oxygen
Corrosion Rate
Intergranular Corrosion

20. ABSTRACT (Continue on reverse side if necessary and identify by block number)

An electrochemical investigation was conducted on the effects of varying the chloride and dissolved oxygen concentration on the corrosion rate of 1020 steel in a saturated calcium hydroxide solution. This solution was intended to simulate the conditions in marine reinforced concrete. The rate and mode of attack were studied electrochemically and microscopically. The electrochemical methods used were the Immersion Mass Loss (IML) Method,

DD FORM 1 JAN 73 1473 EDITION OF 1 NOV 65 IS OBSOLETE
S/N 0102-014-6601

SECURITY CLASSIFICATION OF THIS PAGE (When Data Entered)

the Linear Polarization Method (LPM), the Potentiodynamic Polarization (PDP) Method, and the Potentiostatic Polarization (PSP) Method. The rates of corrosion obtained by each method were correlated to determine the corrosion rate of reinforcing steel in marine reinforced concrete. Microscopic examinations were made, using optical and scanning electron microscopy, to determine the mode of attack and the distribution of corrosion products.

Approved for public release; distribution unlimited.

An Electrochemical Investigation of Corrosion Rates For 1020 Steel In Environments Which Simulate Conditions in Marine Reinforced Concrete

by

Dale Randolph Scott
Lieutenant United States Navy
B.S., University of New Mexico, 1975

Submitted in partial fulfillment of the requirements for the degree of

MASTER OF SCIENCE IN ENGINEERING SCIENCE

from the

NAVAL POSTGRADUATE SCHOOL
June 1981

Author: Dale Randolph Scott

Approved by: Jeff Perkins
Thesis Advisor

Richard A. Reinhardt
Second Reader

R. J. Marto
Chairman, Department of Mechanical Engineering

William M. Tolles
Dean of Science and Engineering

ABSTRACT

An electrochemical investigation was conducted on the effects of varying the chloride and dissolved oxygen concentration on the corrosion rate of 1020 steel in a saturated calcium hydroxide solution. This solution was intended to simulate the conditions in marine reinforced concrete. The rate and mode of attack were studied electrochemically and microscopically. The electrochemical methods used were the Immersion Mass Loss (IML) Method, the Linear Polarization Method (LPM), the Potentiodynamic Polarization (PDP) Method, and the Potentiostatic Polarization (PSP) Method. The rates of corrosion obtained by each method were correlated to determine the corrosion rate of reinforcing steel in marine reinforced concrete. Microscopic examinations were made, using optical and scanning electron microscopy, to determine the mode of attack and the distribution of corrosion products.

TABLE OF CONTENTS

LIST OF TABLES

LIST OF FIGURES

LIST OF SYMBOLS AND ABBREVIATIONS

a	ANODE
Ar	ARGON
c	CATHODE
$CaCl_2$	CALCIUM CHLORIDE
$Ca(OH)_2$	CALCIUM HYDROXIDE
Cl^-	CHLORIDE ION
E	OXIDATION POTENTIAL, VOLTS
E_{app}	APPLIED POTENTIAL
E_{corr}	CORROSION POTENTIAL
ethanol	ETHYL ALCOHOL
F	FARADAY'S CONSTANT, 9.64848×10^4 COULOMBS/EQUIVALENT
i	CURRENT DENSITY, CURRENT/UNIT AREA
i_{corr}	CORROSION CURRENT DENSITY
I_{corr}	CORROSION CURRENT
IML	IMMERSION MASS LOSS
LPM	LINEAR POLARIZATION METHOD
m	METER
mdd	MILLIGRAMS PER SQUARE DECIMETER PER DAY
mm	MILLIMETERS, 10^{-3} METERS
mpy	MILS PER YEAR
mV	MILLIVOLTS, 10^{-3} VOLTS
N_2	MOLECULAR NITROGEN
O_2	MOLECULAR OXYGEN

PDP	POTENTIODYNAMIC POLARIZATION
ppt	PARTS PER THOUSAND
PSP	POTENTIOSTATIC POLARIZATION
SCE	SATURATED CALOMEL ELECTRODE
SHE	STANDARD HYDROGEN ELECTRODE
SEM	SCANNING ELECTRON MICROSCOPE
UNC	UNIFIED NATIONAL COARSE THREAD
μA	MICROAMP, 10^{-6} AMPS
ø	REDUCTION POTENTIAL

ACKNOWLEDGEMENTS

I wish to express my sincere appreciation to Professor Jeff Perkins for stimulating my interest in the field of corrosion engineering and for his guidance in the editing of this thesis; and to Professor R.A. Reinhardt for introducing me to the field of corrosion and providing the additional chemistry background necessary to carry out this research.

I also wish to thank Ms. Andrea McDonald for her timely assistance in gathering the material necessary for the experimental set-ups and for her advice in the performance of preliminary experiments.

I. INTRODUCTION

A. BACKGROUND

Marine reinforced concrete is used extensively in the construction of piers, bridges, pilings, and numerous other structures which are exposed to an ocean environment. One of the most recent applications has been in the construction of deep water oil production platforms deployed in the North Sea [1]. In the past 20 years, it has become apparent that corrosion of the steel reinforcing bars (rebar) in these structures is a serious problem; one which can lead to early failure, within 3-5 years, of structures which are normally expected to have a service life of 30-50 years [2]. Damage is imparted to these structures when the corrosion product creates expansive forces within the structure which result in cracking or spalling.

The problem of rebar corrosion is not limited to structures exposed to marine environments and is in fact a major problem facing highway engineers in the United States. In this case, the problem is aggravated by the application of de-icing salts to highways and bridges during the winter months to keep them clear of ice and snow. Recent estimates indicate that it would cost $12.5 billion to repair or replace bridges of the Federal Highway System that have been damaged due to rebar corrosion. This

estimate rises to $100 billion when bridges off the federal system are included [3].

While repairs in highway applications are difficult, the degree of difficulty becomes many times greater when the repairs must be made on submerged or partially submerged structures. Divers or submersibles are usually involved at a great expense, and the soundness of the repaired areas is sometimes questionable.

The degree of damage to structures in marine applications varies with geography and in most cases with the degree of exposure to the corrosive atmosphere (seawater). The degree of exposure of marine structures to seawater varies from complete submergence, to regions in tidal or splash zones, to regions which are alternately wet and dry due to spray or mist. Typically, the area that sustains the greatest amount of damage is that exposed to tidal action or the splash of waves. For example, investigation of a 35 year old fort, which had been constructed off the coast of England toward the end of World War II, showed corrosion and a loss of concrete cover, due to spalling, only in the splash zone [4].

B. THE PROBLEM

The environment in concrete is normally very alkaline ($pH \geq 12.0$) and tends to passivate the steel. However, the presence of chlorides reduces the passivity by lowering the

pH slightly and breaking down the passive film, thus making the corosion of the rebar more probable. The presence of chlorides may be intentional, as with $CaCl_2$ used to accelerate the setting and strengthening of concrete; or may be due to diffusion of chlorides through cracks in the concrete.

Cracking may occur in concrete due to shrinkage while curing, improper curing techniques, or applied stresses. While limited cracking is acceptable in reinforced concrete, the crack width is carefully controlled to a maximum of about 0.3 mm. Cracks may also serve as the path of ingress for oxygen, thus increasing the likelihood that corrosion of the rebar will take place. This is not to say that the concrete must be cracked in order for seawater, with chlorides and oxygen, to permeate to the rebar. The natural permeability of concrete is on the order of 10^{-10} m/sec; and in deep water applications, where hydrostatic pressure will aid the diffusion process, seawater can permeate to the rebar in about one year.

Another significant factor in reinforced concrete which leads to corrosion of the rebar is the presence of voids in the concrete near the rebar [5]. These may be due to shrinkage or improper compaction of the concrete around the rebar. Thus, there are areas of the rebar left unprotected by the passive film normally formed by the high pH concrete and these unprotected areas become very susceptible to localized

attack. With the knowledge that chlorides and oxygen can diffuse through concrete, D.A. Lewis [6] formulated the following as a model for the basic electrochemical cell responsible for corrosion of steel in concrete.

Steel (Anode)	Concrete relatively permeable and therefore of low pH	Concrete relatively impermeable and therefore of high pH	Steel (Cathode)

The term low pH in the left side of the cell is not meant to imply that the pH is lowered drastically, but only that the interaction of water and chlorides will tend to lower the pH nominally, perhaps 1 pH unit.

When corrosion does occur at the rebar, damage is imparted to the structure when the corrosion product, which is less dense than the base metal and two-four times more voluminous, forms and thus creates tensile stresses within the concrete [7]. These stresses result in cracks which propagate to the surface of the structure and eventually lead to spalling of the concrete cover in the vicinity of the active corrosion sites. Figure 1 shows, schematically, how this process occurs. Figure 2 shows a reinforced concrete seawall that has experienced cracking and spalling typical of the damage seen, due to corrosion of rebar.

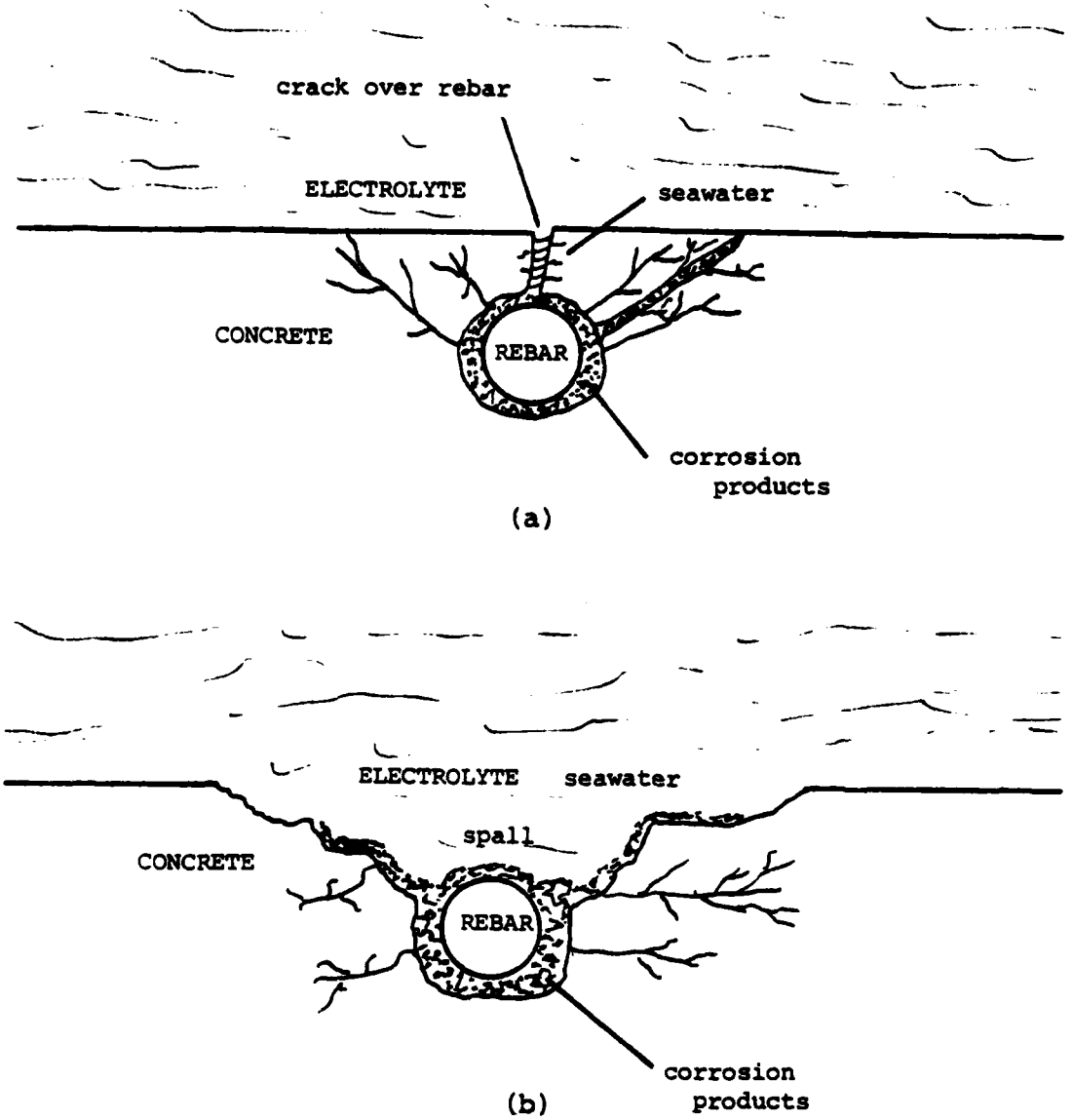

Figure 1. Creation of a Spall

(a) The initial crack over the rebar initiates the corrosion process and cracking has started.

(b) Several cracks propagated to the surface, spalling the concrete cover, corrosion and cracking continues.

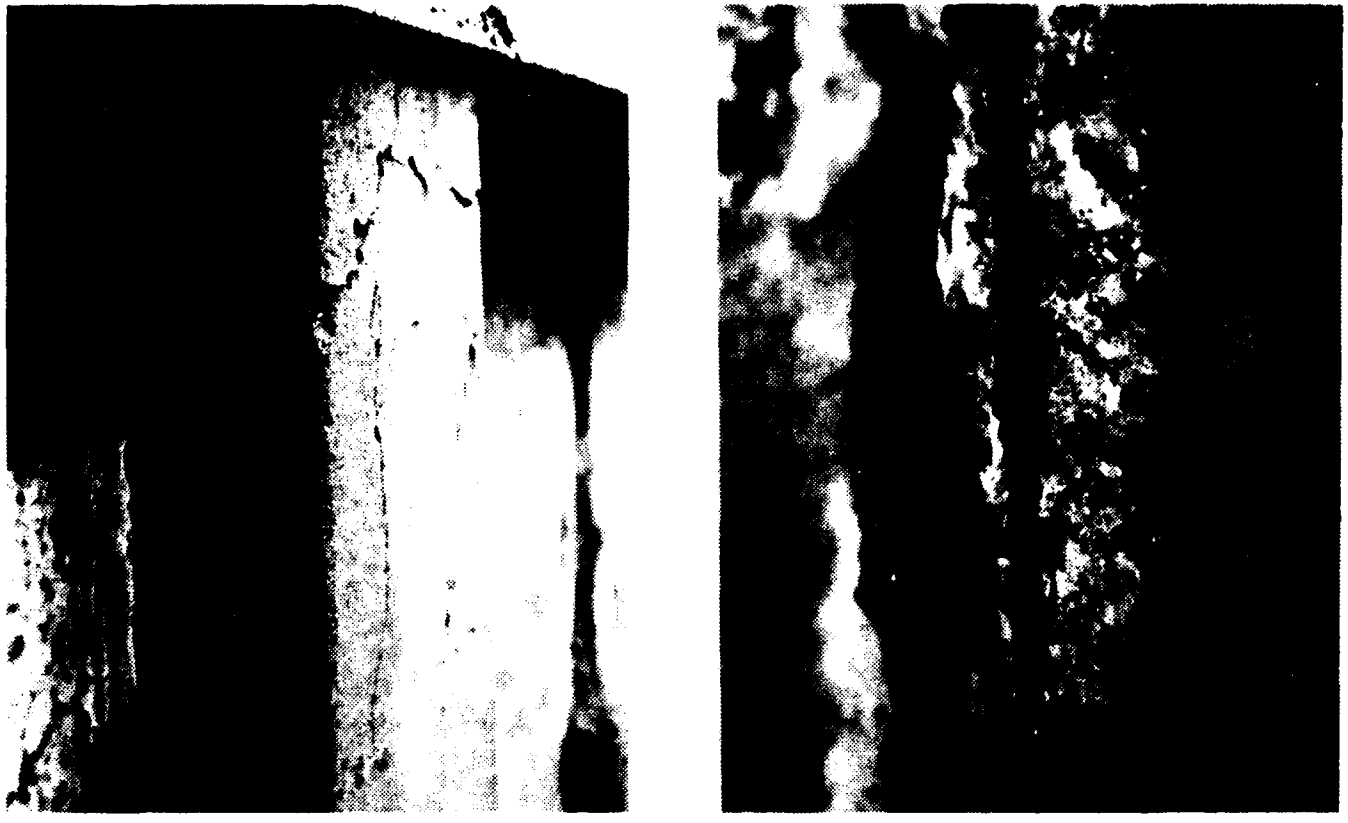

(a) (b)

Figure 2. Seawall showing damage typical of that incurred when steel reinforcing bars corrode. Note the cracks running parallel to the lay of the rebar in (a) and the regions of spalling in (b).

C. PREVIOUS STUDIES -- AN OVERVIEW

The deterioration of reinforced concrete due to corrosion of steel reinforcing bars has only recently (within the past 20 years) been recognized as a serious problem that must be recognized and considered in future structures by structural and design engineers [8]. The search for methods to reduce or eliminate the corrosion of steel in concrete has taken many paths. Perhaps because concrete is used extensively throughout the world in the fabrication of structures (usage in the United States alone was about 80 million tons in 1976 [9]), the cement and concrete industry has invested much time and research into the problem of imbedded metal corrosion. The investigations by the cement and concrete industry have included additions or changes in the composition of the cement used, the effects of size and composition of aggregates, the use of admixtures, the effects of varying the water/cement ratio, and the effects of variables in construction techniques [10, 11, 12, 13, 14]. Industry representatives have also been involved in research to determine the mechanisms and effects of corrosion on reinforced structures.

The Federal Highway Administration, as well as the highway departments of many states, has also expended a great deal of time and effort into developing methods of detecting rebar corrosion in bridges and highways as well as methods of preventing and/or protecting highways and bridges from

rebar corrosion. Elaborate electrochemical techniques have been developed [15, 16, 17] to monitor the corrosion process in structures and cathodic protection is being installed in many new or reconstructed structures [18, 19, 20].

Much research has also been done on the factors which affect the corrosion of steel in concrete. The effects of moisture content [21, 22] of the concrete and the use of inhibitors in concrete mixes [23, 24] as well as the effects of sulphate ions and stress [25] have been investigated. Investigations into methods of protection have included cathodic protection [26, 27], metallic and non-metallic coatings for rebar [28, 29], coatings for the concrete [30], and the impregnation of concrete with wax or polymers to create an impermeable seal [31].

The ability to remotely monitor a reinforced structure for active corrosion is another area that has received a great deal of attention. Significant progress has been made in an effort to define a range of electrode potentials which corresponds to a very high probability, >95%, that the rebar is actively corroding [32,33]. This work is based on the fact that a passive film forms on the rebar initially, due to the high pH of the concrete, and the breakdown of this film corresponds to a rapid change to a more anodic (active) potential. The characteristic potential beyond which this action occurs is known as the Flade potential, which for iron is given by:

$$E_F = -0.63 + 0.059\ pH \quad [1] \qquad (1)$$

The penetration of chlorides to the rebar tends to depassivate the environment and break down the passive film. Gjørv and Vennesland [34] and others [35] have shown that the diffusion of chlorides into concrete occurs readily and it is just a matter of time before the chlorides penetrate to the rebar. It was also shown that the depth of penetration is a function of the water/cement ratio of the concrete only for a narrow surface layer, after which the diffusion rate is governed by the quality of the concrete.

The other major factor for active corrosion of rebar is the presence of oxygen. Again, Gjørv et. al. [36] have shown that the diffusion of oxygen through concrete occurs readily and the rate of diffusion is affected only by the quality of the concrete. Increasing the thickness of concrete covering the rebar does not decrease the diffusion time as might be expected, as the thicker cover serves only to increase the flux of oxygen diffusion through the concrete.

The thrust of the research presented in this thesis is to provide additional information on the rate at which steel reinforcing bars corrode in concrete as a function of various chloride and dissolved oxygen concentrations. Information is also presented on the distribution of corrosion products and mode of attack.

---

[1] Uhlig, Corrosion and Corrosion Control, p. 64.

II. DETAILS OF EXPERIMENTAL METHODS

The determination of corrosion rates by electrochemical methods was performed on specimens of 1020 steel in a saturated calcium hydroxide, $Ca(OH)_2$, solution of varying Cl^- and O_2 concentrations. The corrosion rates were determined by the methods described below. In addition to the rate determinations, microscopic examination of specimens was performed to determine the distribution characteristics of the corrosion product and the modes of attack. This work was carried out by light and scanning electron microscopy.

A. THE COUPON IMMERSION MASS-LOSS (IML) METHOD

1. Test Coupons

Test coupons were machined from 1020 steel rods all taken from the same lot of steel (provided by Civil Engineering Laboratory, Port Hueneme, CA). Each coupon was a right circular cylinder; 0.5 inches in diameter, 0.25 inches high, with a 3-48 UNC thread tapped in one end. (See Figure 3.)

The exposed surface area of the test coupon was approximately the same for all runs, about 0.785 in^2. Coupons were finished to a 3/0 surface with metallurgical polishing paper, cleaned with acetone, ultrasonically cleaned in ethanol, and dried with a warm air blower. Coupons were stored in a desiccator until needed. Test coupons were

accurately measured, weighed on an analytical balance, attached to a specimen holder, and placed in the electrolyte of choice.

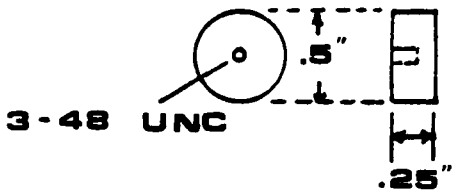

Figure 3. Corrosion Test Coupon

2. IML Corrosion Cell

The IML test cell was a 1000 ml round bottomed, three-necked flask. These were arranged in an acrylic fixture designed to hold twelve such cells. The fixture was immersed in a constant temperature bath at 20 ± 0.1°C. Each flask was fitted with a Graham condenser, a gas dispersion tube, and a specimen holder. (See Figure 4.) The specimen holder was arranged so as to allow total immersion of the test coupon throughout the test run.

Each specimen holder was fitted with a teflon compression seal to prevent a bi-metallic couple between the coupon and the internal metal holder. The gas dispersion stones were attached to a cylinder of compressed gas to control the dissolved O_2 content of the electrolyte.

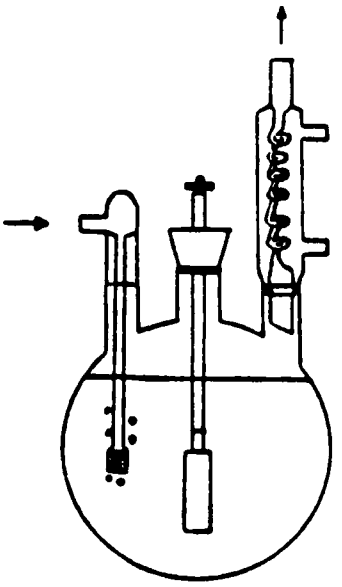

Figure 4. A typical IML corrosion cell including from left to right a gas sparger, the test coupon holder, and the Graham condenser.

3. Electrolyte

Specimens were subjected to a 28 day immersion test in saturated solutions of $Ca(OH)_2$. Variables in the electrolyte were the Cl^- and O_2 concentrations. Chloride ion concentrations of 5, 19, or 30 parts per thousand were used, and dissolved O_2 concentration was varied from approximately 0 ppm to 20 ppm.

4. The IML Experiment

After addition of the appropriate electrolyte to each flask, it was placed in the holding fixture and placed in the constant temperature bath. The corrosion cells were then fitted with dispersion stones, Graham condensors and a stopper in place of the specimen holder. Gas flow was started and allowed to purge through the electrolyte overnight. The coupons were then placed on holders and inserted into the center neck of the corrosion cell. Starting time, pH, and dissolved oxygen levels were noted and record sheets started for each cell.

All corrosion cells were periodically monitored, (when LPM measurements were taken) for electrolyte pH and O_2 levels. These were recorded to demonstrate constancy of test conditions in the immersion experiments.

At the end of the IML experiment (28 days), coupons were removed from the corrosion cell, lightly rinsed with distilled water, and allowed to dry with the corrosion products intact. Selected coupons were examined by light microscopy or scanning electron microscope before and after corrosion products were removed. All coupons were carefully scraped, scrubbed with a stiff brush in running water, ultrasonically cleaned, and dipped in cold acid to remove the corrosion products. After rinsing with distilled water and acetone, coupons were dried by a warm air blower and weighed on an analytical balance. Mass losses were

recorded and converted to corrosion rates. Figure 5 is a schematic representation of the IML test set-up.

5. Equipment Used -- IML Method

- 1000 ml 3 necked flasks
- Gas dispersion tubes
- Graham condensors
- Specimen holder
- Forma Temp Constant Temperature Bath and Circulator
- Acrylic Cell holding fixture
- Compressed gas - Ar, N_2, O_2, Dry Air
- 1020 Steel coupons
- Sartorius, Type 2403 Analytical Balance
- Beckman Research PH Meter Model 1019
- Beckman Zeromatic PH Meter
- Markson PH Meter, Model 4403
- Lazar Dissolved Oxygen Probe Model, DO-166

B. THE LINEAR POLARIZATION METHOD (LPM)

1. The LPM Experiment

At predetermined intervals the linear polarization resistance was measured using the three-electrode method [37] over a range of $\pm$ 20 mV with respect to E_{corr} measured. By making the LPM measurements on the IML test coupons, instantaneous rates were obtained without significantly perturbing the corrosion processes at play in the cells. (See Figure 6.)

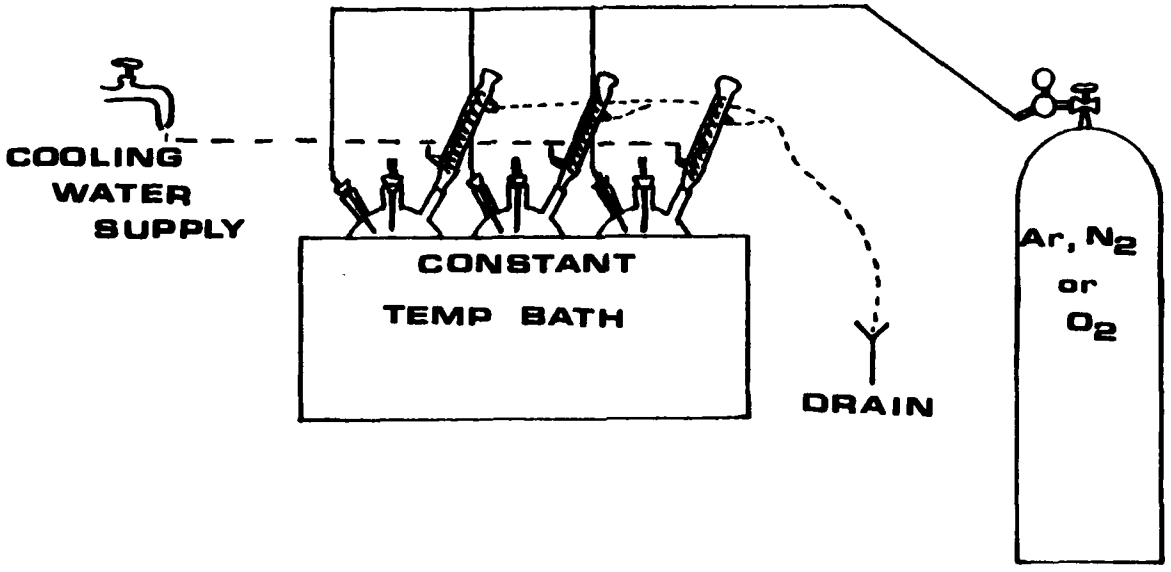

Figure 5. Test Set-Up for IML Corrosion Measurements

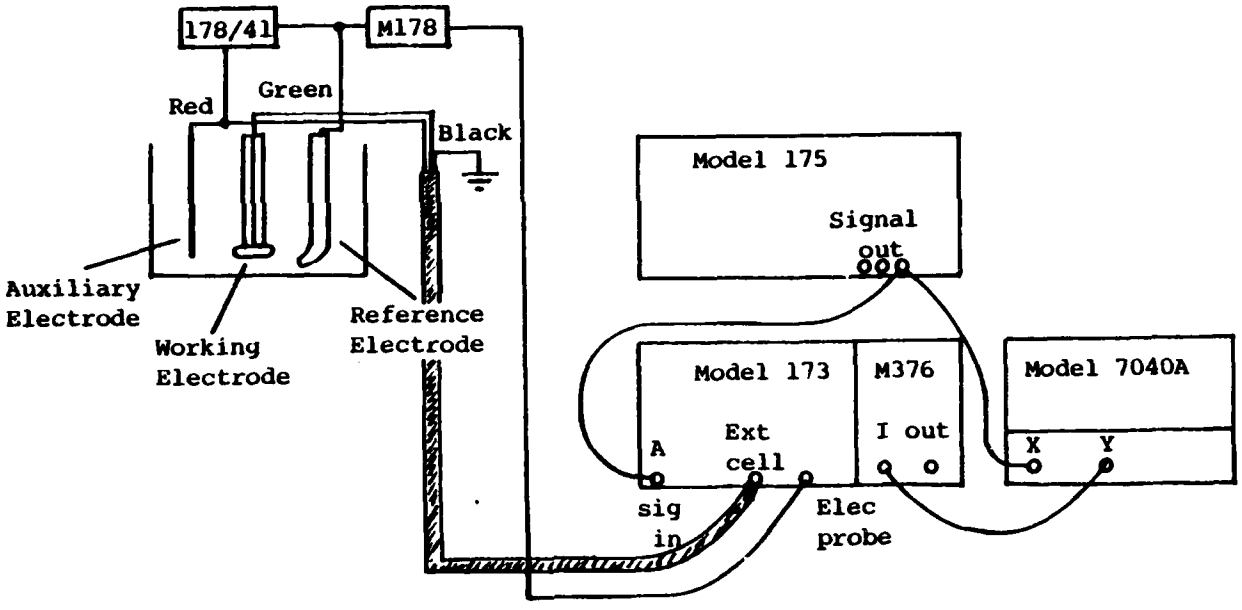

Figure 6. Test Set-Up for LPM Corrosion Measurements

2. Equipment Used - LPM

- Corrosion Cell of IML test
- Princeton Applied Research Model 173
  Potentiostat/Galvanostat
- Princeton Applied Research Model 175
  Universal Programmer
- Hewlett-Packard, Model 7040 A
  X-Y Recorder

C. POTENTIODYNAMIC POLARIZATION METHOD (PDP)

1. PDP Test Coupons

Test coupons were of the same geometry and size as those used in the IML tests, or were mounted in acrylic plastic as shown in Figure 7.

Figure 7. Modified Test Coupon - Mounted in Acrylic Plastic

2. PDP Corrosion Cell

The test cell was a 1000 ml, 5 necked flask fitted with two high density graphite auxiliary electrodes, a gas sparger, a Lugin probe-salt bridge and a specimen holder in the middle neck. The corrosion cell is shown in Figure 8. Figure 9 shows the specimen holder in detail.

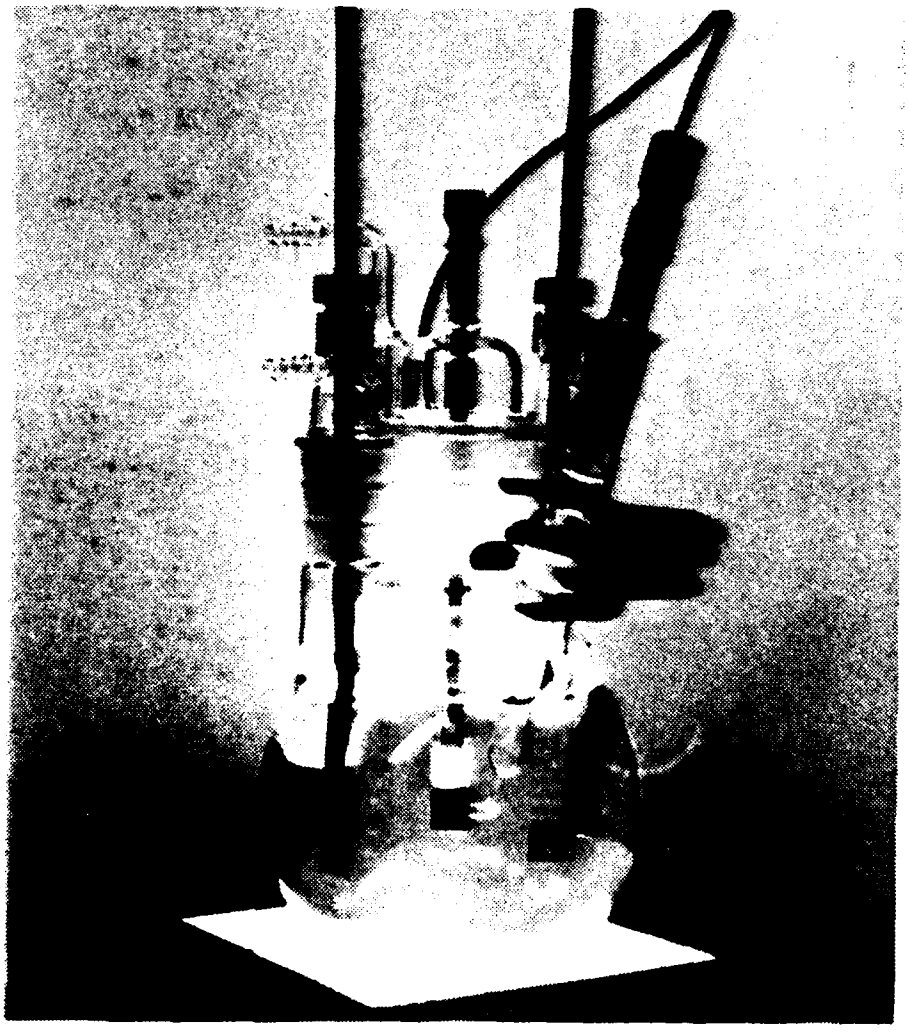

Figure 8. Corrosion Cell Used in PDP and PSP Tests

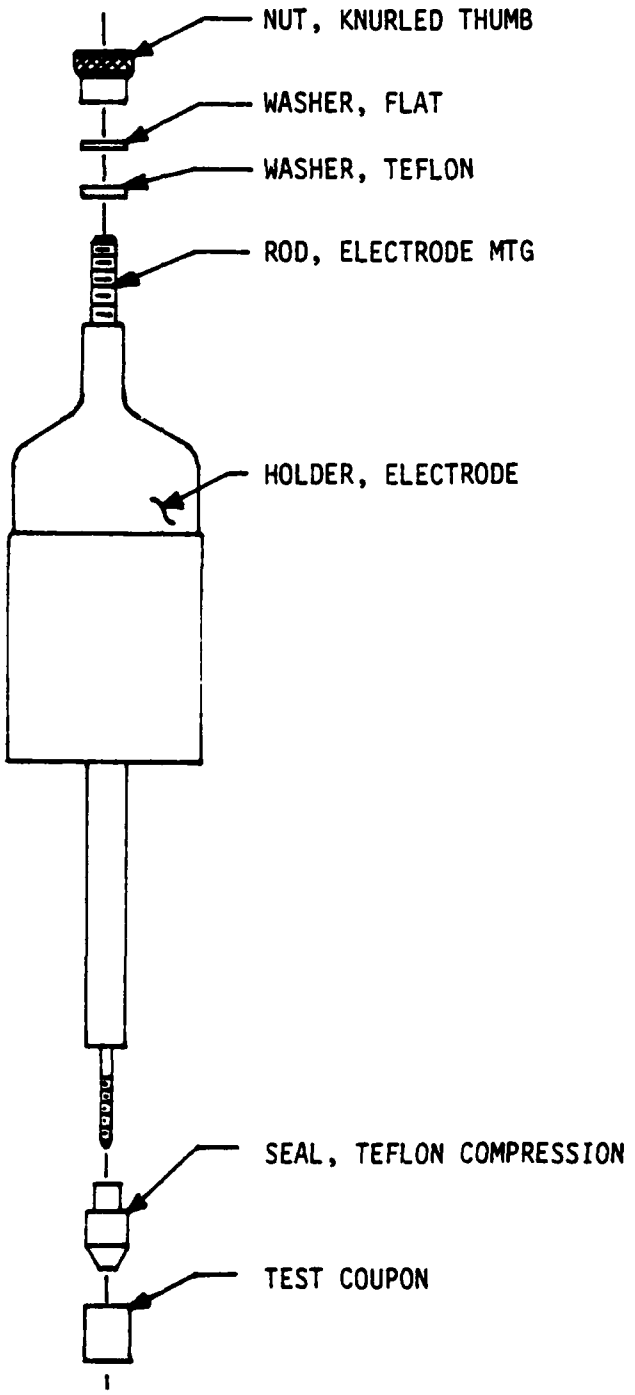

Figure 9. Detail of PDP Specimen Holder

3. The PDP Experiment

The test coupon was immersed in the electrolyte, after the solution had been stirred and aerated with the appropriate purge gas for about ten minutes. Gas flow was then reduced, the stirrer stopped, and the specimen inserted, making certain that any adhering bubbles were shaken loose from the coupon. Electrode leads were attached and corrosion potential measured. When the coupon was freely corroding in the electrolyte (indicated by a stable E_{corr}), the corrosion potential was recorded along with pH, temperature, and dissolved oxygen content. Starting at this potential, the potential was scanned at 0.2 mV/sec in the cathodic direction for about 200 mV at which point the scan direction was reversed and terminated at a potential about 800 mV more positive than the lower limit. The resultant plot of log current vs. potential comprises a complete potentiodynamic curve for the given test coupon and solution. The features of the curves produced were noted and compared to those produced by other specimens. The plots were then analyzed, where possible, by standard methods to compute i_{corr}, E_{corr}, and the corrosion rates for the test coupon. Figure 10 shows the PDP test set-up.

4. Equipment Used - PDP

- 1000 ml, 5 neck Flask
- Princeton Applied Research Model 173 Potentiostat/Galvanostat

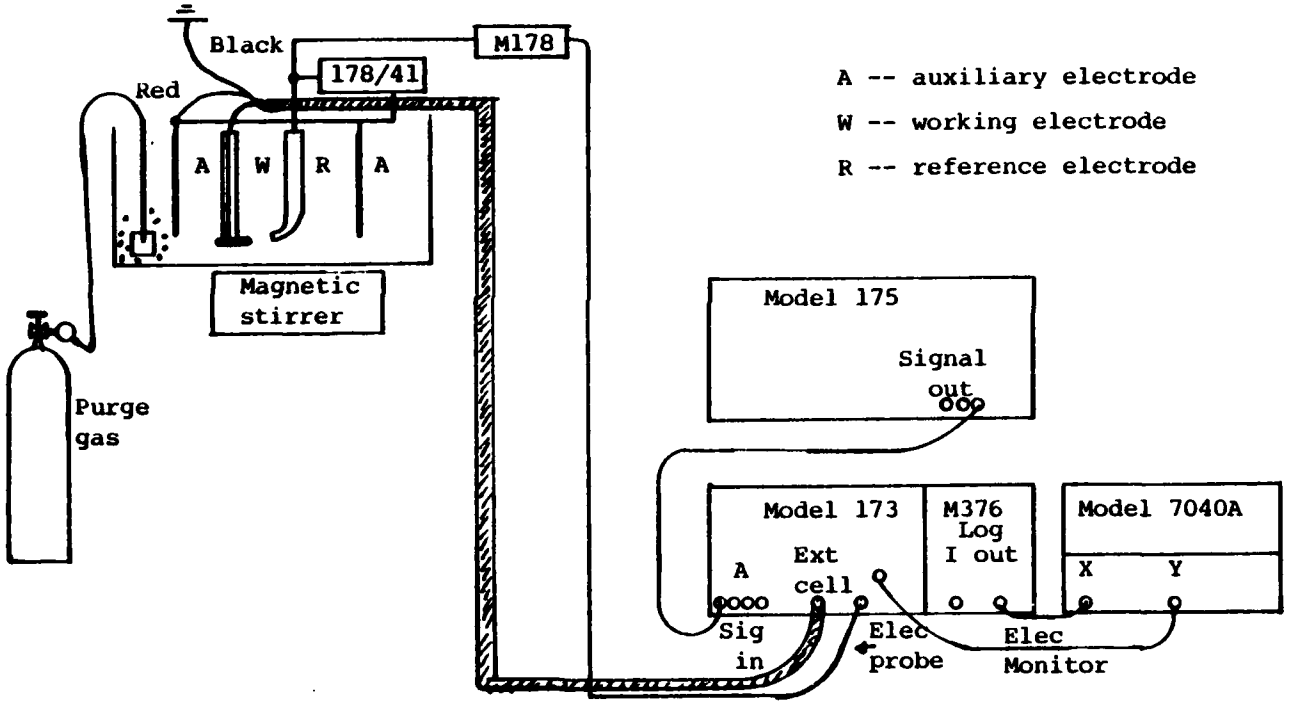

Figure 10. Test Set-Up for PDP Corrosion Measurements

- Princeton Applied Research Model 175 Programmer
- Hewlett-Packard Model 7040A X-Y Recorder
- Compressed Gas - Ar, N_2, O_2, Dry Air
- Beckman Research PH Meter Model 1019
- Markson PH Meter, Model 4403
- Lazar Dissolved Oxygen Probe Model DO-166
- Beckman Zeromatic PH Meter

D. POTENTIOSTATIC POLARIZATION METHOD (PSP)

1. PSP Test Coupons

Test coupons used for these experiments were of the same material and geometry as those used in previous experiments. Coupon preparation was the same as in PDP tests.

2. PSP Corrosion Cell

The same type of cell and electrical hookups as used in the PDP tests was used for these tests.

3. The PSP Experiment

As in the PDP tests, the electrolyte of choice was well aerated and stirred prior to introduction of the test coupon which was then allowed to come to E_{corr}. At this point a potential 50 mV more positive than E_{corr} was applied for a fixed length of time. This forced the specimen to act as an anode and therefore to oxidize. Standard runs times of 12, 60, 180, and 720 minutes were used. Current was recorded as a function of time on a strip chart recorder, using the current-output jack on the current-to-voltage

module of the potentiostat. Following the longer runs, specimens were lightly rinsed with distilled water and dried with a warm air blower prior to microscopic examination of selected test coupons. The amount of material oxidized was then calculated from the area under the current-time plot by graphical integration and then applying Faraday's Law:

$$\text{mass lost} = (e/F) \int I \, dt \qquad (2)$$

where e is the equivalent weight of the metal in grams per equivalent (atomic weight, in grams, divided by the number of electrons participating in the redox reaction). $\int I \, dt$ is the current-time integral in ampere-seconds (coulombs), and F is the Faraday constant, 9.64846×10^4 coulombs/equivalent. The result of the calculation is the mass loss in grams, assuming soluble reaction products and/or exact scraping off of insoluble products.

4. Equipment Used - PSP

   - Same as used in PDP tests
   - Strip chart recorder substituted for X-Y recorder

E. MICROSCOPIC EXAMINATION

1. Light Microscopy

Selected specimens were examined using a Zeiss photomicroscope at magnifications up to 100X to determine corrosion product distribution characteristics. Specimens were placed in an acrylic holder to minimize disturbance of the corrosion products during examination.

2. Scanning Electron Microscopy

Selected specimens were further examined using the Cambridge S4-10 scanning electron microscope to determine corrosion product distribution and the mode of attack. Magnifications up to 20,000X were used to examine the test coupons. Depending on the surface to be examined, the test coupons were mounted mechanically via the threaded hole in the coupons or by using colloidal silver to attach the coupon to the mounting stub.

F. CONTROL OF ELECTROLYTE CHEMISTRY

1. pH

Numerous preliminary experiments were performed in an effort to establish a reliable and controllable procedure for varying the pH of the electrolyte while maintaining the desired concentrations of Cl^- and dissolved oxygen. In each case it was found that the pH established by the desired Cl^- concentration could not be changed without de-saturating the electrolyte with respect to calcium hydroxide. A wide range of pH values for concrete, 11.0 to 13.5, have been reported [38], but in these instances the electrolyte was much more complex than a saturated solution of calcium hydroxide. In this study, pH was found to be affected by the chloride concentration and thus three pH levels corresponding to the three chloride concentration levels were observed. At 5 ppt Cl^- the pH of the electrolyte approached

that of saturated calcium hydroxide, about 12.40. The pH for a Cl^- concentration of 19 ppt was 12.20 and the pH for a Cl^- concentration of 30 ppt was 12.00

2. Dissolved Oxygen Concentration

The dissolved oxygen concentration of the electrolyte was varied from about 0 ppm to an intermediate value of 5.5 to 6.5 ppm to a level of super-saturation, about 20 ppm. The dissolved oxygen level was controlled by purging the electrolyte with compressed gas, Ar, N_2, O_2, or Dry Air, to obtain the desired oxygen content.

3. Chloride (Cl^-) Concentration

The chloride ion (Cl^-) concentration was controlled by mixing calcium chloride, $CaCl_2$, with distilled water. Calcium chloride was used to introduce the Cl^- since it is frequently used to accelerate the development of strength of concrete while it is setting and is also applied to the surface as a curing agent [39]. The use of calcium chloride also precluded the introduction of other elements which might react during the corrosion process. Electrolytes with a Cl^- concentration of 5, 19, and 30 ppt were prepared (see Appendix C for details) for each method of testing.

G. CORROSION PRODUCT REMOVAL

The corrosion products were removed from test coupons prior to final weighing of IML test coupons, to determine mass loss, and prior to scanning electron microscope

examination of selected test coupons. The corrosion products were carefully scraped off and the test coupon scrubbed with a stiff brush under running water. The test coupons were then placed in a beaker of cold acid in the ultrasonic cleaner to remove any remaining corrosion products. The acid used for final cleaning of test coupons was

50 ml HCl + 50 ml H_2O + 0.2 g Hexamethylenetetramine .

The test coupons were immersed for 15 second intervals until clean and immediately rinsed with ethanol to stop the action of the acid.

III. RESULTS

A. AS COMPARED TO AN ELECTROCHEMICAL MODEL

Concrete is a complex chemical medium. As such it presents several problems in constructing a model which adequately describes the electro-chemical processes which occur as imbedded steel rebar corrodes. The model must consider the diffusion of oxygen and chlorides through the concrete, the chemical reactions characterizing the formation of corrosion products, and the current flow in the electrochemical cell formed by the steel rebar and the concrete. Z.P. Bazant [40] has formulated just such a model, which in its entirety is an initial-boundary-value problem of 13 equations and 13 unknowns which can be solved by the finite element method with the aid of a computer. As this research was performed using an environment which simulates that of marine reinforced concrete, only that portion which characterizes the chemical reactions was used. The essence of this approach is an attempt to correlate predicted open circuit potential differences with the potentials and corrosion rates obtained experimentally.

The electrochemical processes leading to the corrosion of rebar in concrete are summarized as follows:

a. At the anode, the passive film is broken down by the presence of Cl^- leading to the dissolution of iron:

$$Fe \rightarrow Fe^{++} + 2e^{-} \quad (3)$$

b. The cathodic reaction requires diffusion of oxygen through the concrete and is given by:

$$O_2 + 2H_2O + 4e^{-} \rightarrow 4OH^{-} \quad (4)$$

c. Near the anodic surface, the Fe and OH^{-} react to form ferrous hydroxide; so that the electrode reaction becomes:

$$2Fe(OH)_2 + 2e^{-} \rightarrow Fe(s) + 2OH^{-} \quad (5)$$

d. The total cell reaction, from equations 3-5 is:

$$2Fe + 2H_2O + O_2 \rightarrow 2Fe(OH)_2 \quad (6)$$

e. The ferrous hydroxide further reacts with available oxygen and water to form hydrated red rust ($Fe\ O\ OH + H\ O$), according to:

$$4Fe(OH)_2 + O_2 + 2H_2O \rightarrow 4Fe(OH)_2 \quad (7)$$

This is not the only corrosion product formed, but it is the most important since its volume is four times that of the steel from which it is forming. Black rust, Fe_3O_4, is the other corrosion product most commonly formed and its volume is twice that of the steel from which it is formed. While other corrosion products may be found, the reactions relating to the formation of red rust are of primary concern since this is the most dangerous to the structures in terms of the expansive forces generated by the formation of rust.

From the reactions outlined above, it is possible to evaluate the electrode potentials which determine the open circuit potential for the cell. Following is an evaluation of the open circuit potentials predicted by the reactions of equations 3-5. The governing equation for this evaluation is the Nernst Equation

$$\phi = \phi^\circ - \frac{RT}{nF} \ln Q \qquad (8)$$

where ϕ° is the standard electrode potential measured with respect to the standard hydrogen electrode; R is the universal gas constant (8.314 j/°K); T is the absolute temperature in °K; F is the Faraday (96,500 coulombs per equivalent); n is the number of electrons or chemical equivalents taking part in the reaction; and Q is the activity quotient constant (activities of products/activities of reactants). Taking the case where the pH of the electrolyte is 12.5 and the oxygen concentration is 1.0 ppm (2.44×10^{-2} atm) at 25 °C; the anodic reaction, equation (5) is:

$$Fe(OH)_2 + 2e^- \rightarrow Fe(s) + 2OH^-$$

$$\phi^\circ = 0.877 \text{ V}$$

Applying the Nernst Equation

$$\phi_a = \phi^\circ - \frac{RT}{nF} \ln [OH^-]^2$$

$$= -0.877 - \frac{0.0591}{2} \log [OH^-]^2 \qquad (9)$$

$$pOH = 14 - pH$$

$$= 14 - 12.5 = 1.5$$

then, since

$$pOH = -\log[OH^-]$$

$$[OH^-] = 10^{-1.5} = 31.6 \times 10^{-3}$$

Substituting into equation (9) gives

$$\phi_a = -0.877 - 0.0296 \log 31.6 \times 10^{-3}$$

$$= -0.788 \text{ V}$$

The cathodic reaction is

$$O_2 + 4H^+ + 4e^- - 2H_2O$$

$$\phi^\circ = 1.229 \text{ V}$$

$$\phi_a = \phi^\circ - \frac{RT}{nF} \ln \frac{[H_2O]}{[O_2]} - 0.0591 \text{ pH} \qquad (10)$$

$$= 1.229 - 0.0148 \log \frac{1}{2.44 \times 10^{-2} \text{ atm}} - 0.739$$

$$= 0.466 \text{ V}$$

The open circuit potential difference is then

$$\phi_{\text{open circuit}} = \phi_i - \phi_a = 0.466 - (-0.788)$$

$$= 1.254 \text{ V} \qquad (11)$$

This initial condition is shown in Figure 11 by the solid lines which represent the reduction of O_2 and the oxidation of Fe. Lines 1 and 2 represent the reduction reaction for increasing O_2 concentrations at a constant pH. This results in a larger open circuit potential difference and, as shown by the intersection with the Fe-oxidation line, a less

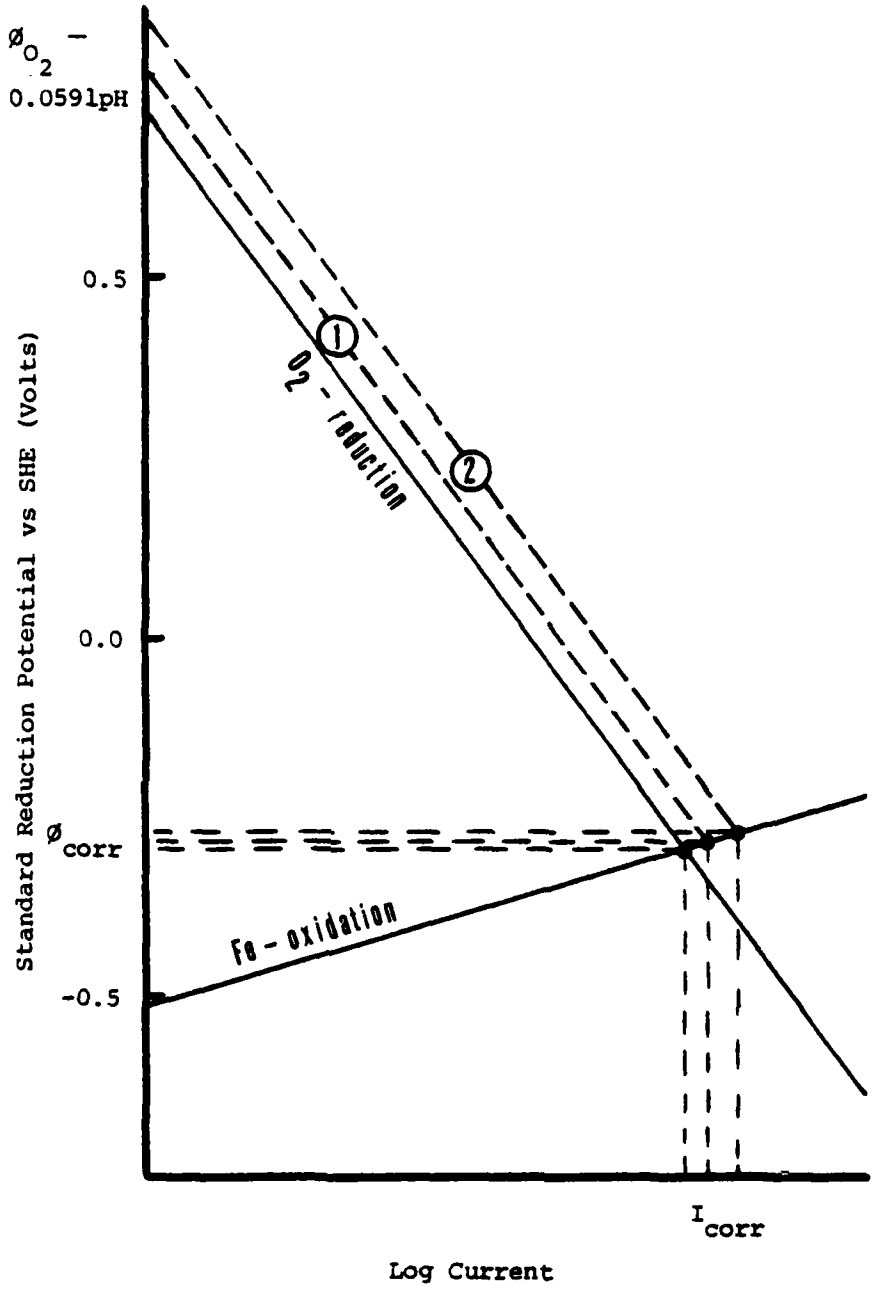

Figure 11. Fe - O_2 Polarization Diagram for Constant pH. Lines 1 and 2 Represent Increases in O_2 Concentration of Electrolyte

negative ϕ_{corr}. This was observed experimentally and the results are summarized in Table I.

Table I: Average ϕ_{corr} (measured) vs SCE as a Function of Oxygen and Chloride Concentrations

O / Cl^-	0 ppm	5.8 ppm	20 ppm
5 ppt	-.502	-.362	-.353
19 ppt	-.538	-.425	-.429
30 ppt	-.551	-.475	-.459

Table I also indicates that as pH is decreased, corresponding to an increase in Cl^- concentration and thus an increase in conductivity, the corrosion potential becomes more negative. This is not readily seen in Figure 11 as a change in pH changes the slope of the Fe-oxidation line as well as that of the O_2-reduction line. The change in corrosion potential can be more readily seen through the use of Ohm's law.

$$E = IR \tag{12}$$

As the concentration of Cl^- increases, conductivity increases and resistance, R, decreases. The increase in

conductivity also results in an increase in current, I, with the net result being an increase in the potential, E. Table II shows the average electrode potentials measured by Abdul Azim [41] and Hausmann [42].

Table II. Average Corrosion Potentials for Mild Steels in Concrete

Electrolyte	pH	O_2 (ppm)	ϕ_{corr} vs SCE
Saturated $Ca(OH)_2$	12.40	N.A.	-0.302 [1]
$Ca(OH)_2$ + 0.01M NaCl	12.10	N.A.	-0.440 [1]
$Ca(OH)_2$ + 0.10M NaCl	11.70	N.A.	-0.530 [1] -0.460 to -0.490 [2]

1. As measured by Abdul Azim.
2. As measured by *Hausmann*

The corrosion potentials and pH values presented in Table II are comparable to the results presented in Table I and Appendix D. Differences can be accounted for by the use of different alloys for the rebar specimens and the use of NaCl rather than $CaCl_2$ as the source of Cl^-. However, the most important point to note here is the trend of increasingly more negative corrosion potentials with increasing chloride levels in the electrolyte. This behavior is predicted by the electro-chemical model and verified by Tables I and II.

The model as used here, offers a method to verify the direction of change of ϕ_{corr}. In cases where trends in

measured values correspond to those predicted by the model, one can compare the measured values of ϕ_{corr} to the Flade potential (Equation 1) or the Pourbaix diagram (see Figure E-1) to predict whether or not corrosion can occur. By this method, a range of electrode potentials that correspond to active corrosion could be established for a range of conditions. This information coupled with the use of electrodes imbedded in the concrete would provide a quick method to monitor the corrosion processes in a structure and facilitate timely corrective action.

B. SUMMARY OF CORROSION RATE DATA

1. IML and LPM Corrosion Rates

The immersion mass loss tests and the linear polarization tests were conducted simultaneously on the same test coupons over a period of 28 days. Table III shows the average corrosion rates measured for the IML tests as a function of oxygen and chloride concentrations.

Table III: Average IML Corrosion Rates as a Function of Oxygen and Chloride Concentrations

O_2 / Cl^-	0 ppm	5.8 ppm	20 ppm
5 ppt	0.63 mdd	15.03 mdd	14.43 mdd
19 ppt	1.16 mdd	11.43 mdd	51.85 mdd
30 ppt	1.44 mdd	19.03 mdd	73.88 mdd

Here it is seen that as the chloride or oxygen concentration increases, the corrosion rate increases. Figures 12, 13, and 14 are the average LPM measurements for IML test coupons. These figures show how the corrosion rate varied as a function of time during the 28 day immersion test, indicating when the corrosion rate was increasing, decreasing, or remaining steady. The general trend noted in these figures is an increase in the corrosion rate with time during the test period. The magnitude of the instantaneous rates also show the same trend, established earlier, with respect to oxygen and chloride concentrations. The curves in Figure 12 start at a rate somewhat higher than the average rate for the remainder of the test due to the introduction of oxygen to the test cell upon initial insertion of the test coupons. The rate rapidly decreased from this point as the oxygen was consumed by the corrosion process. From this point on, the LPM measurements showed a slight increase with time to completion of the IML test. The exception to this behavior was demonstrated for the electrolyte containing 30 ppt Cl^-, the curve for which shows some drastic changes in rate. The implication here is that something has happened, perhaps a breakdown of the passive film or the formation of a pit or some other form of localized attack, which has accelerated the corrosion process for a period of time. The subsequent decrease then implies that a protective film has again been formed thus lowering the corrosion rate. Referring to Figure

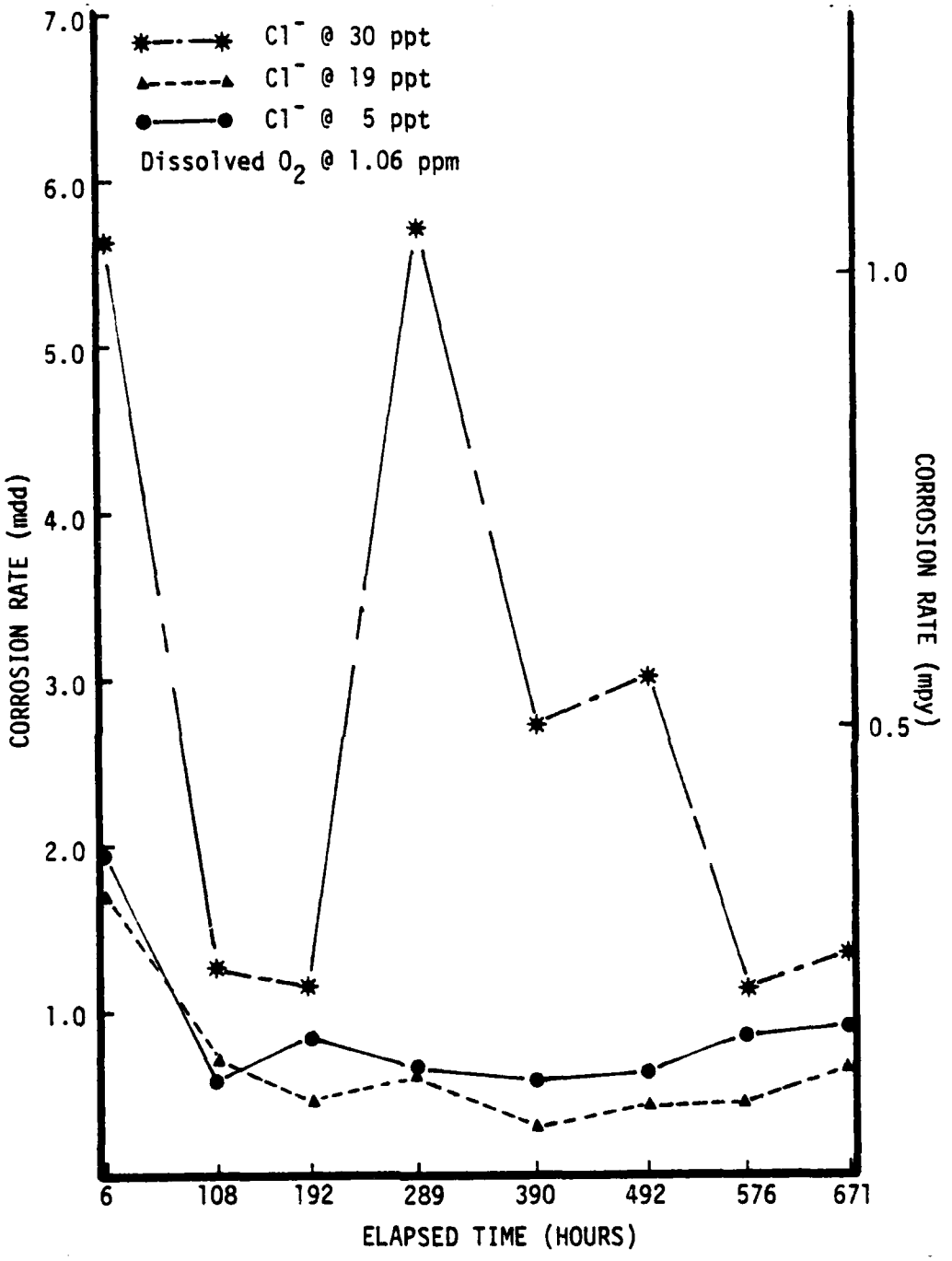

Figure 12. Average LPM Measurements for IML Test Coupons in Electrolytes of 5, 19, and 30 ppt Cl^- and 1.06 ppm O_2. Each Curve Based on Measured Rates for Three Test Coupons.

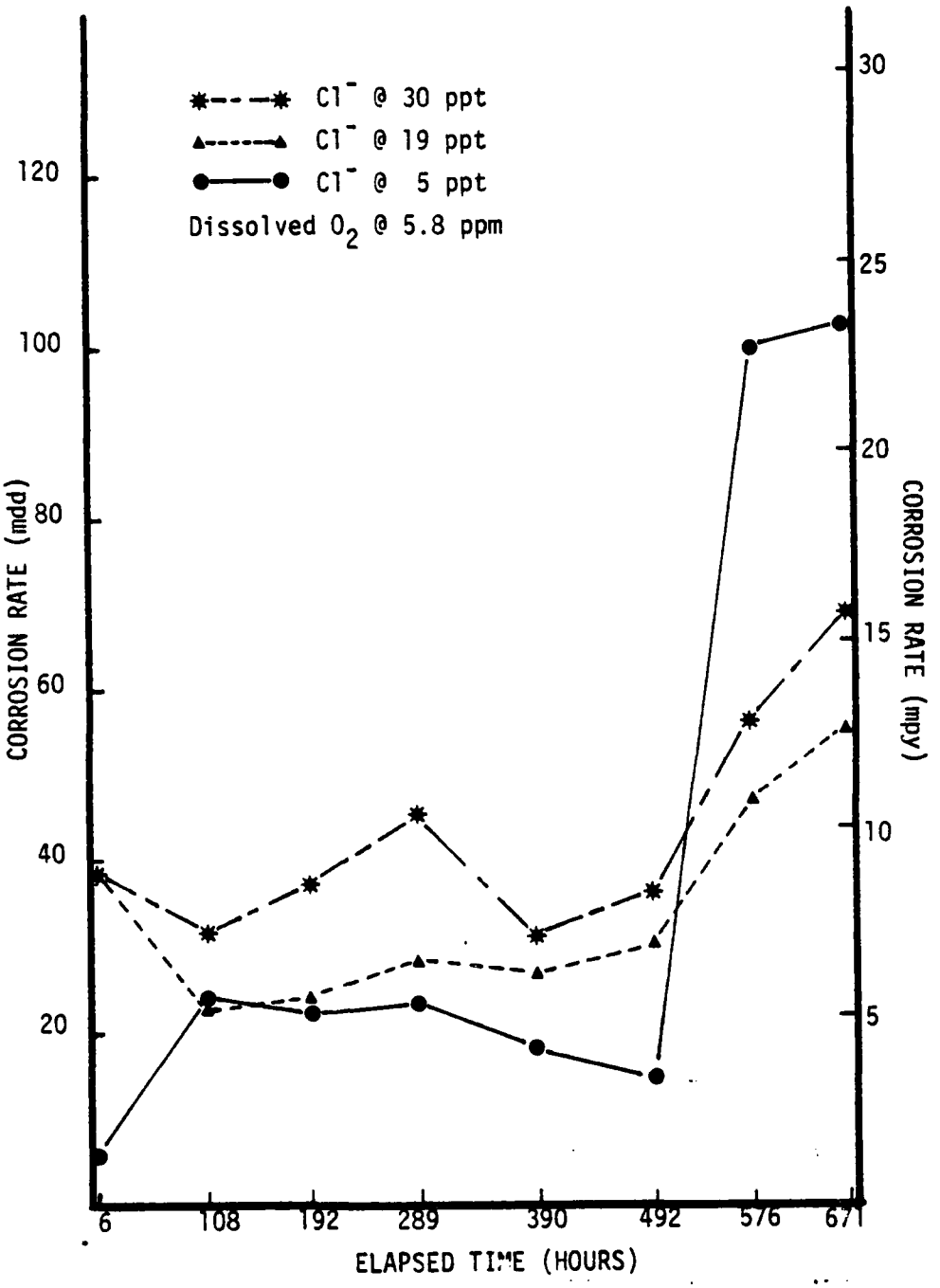

Figure 13. Average LPM Measurements for IML Test Coupons in Electrolytes of 5, 19, and 30 ppt Cl^- and 5.8 ppm O_2. Each Curve Based on Measured Rate for Three Test Coupons.

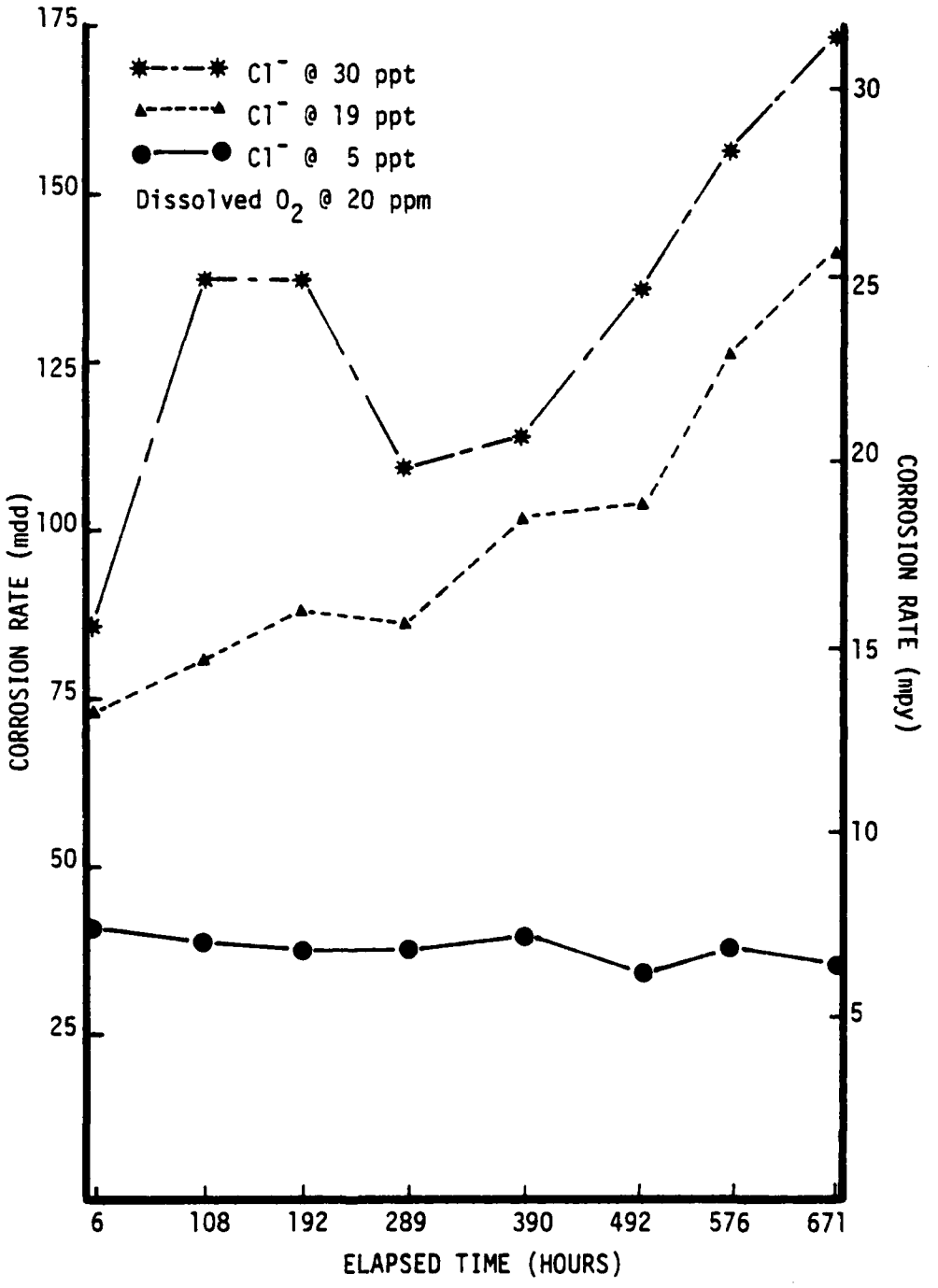

Figure 14. Average LPM Measurements for IML Test Coupons in Electrolytes of 5, 19, and 30 ppt Cl^- and 20 ppm O_2. Each Curve Based on Measured Rates for Three Test Coupons.

13, the rapid increase in the corrosion rate of the test coupons in the electrolyte containing 5 ppt Cl^- was accompanied by the appearance of red rust. The appearance of red rust was quite unexpected, as it had not appeared up until this point except in a few isolated cases. The main difference in this case and those noted earlier was that the corrosion product uniformly covered the entire surface of the test coupon rather than appearing at a localized corrosion site. Unfortunately, neither Bazant's model [43] nor any other know model can predict which corrosion product will form, not its distribution. As noted in Table III, the corrosion rate for the test coupons in the electrolyte containing 5 ppt Cl^- was significantly higher than the rate for those in the electrolyte containing 19 ppt Cl^-. The formation of red rust was not observed on any of the other test coupons; it can only be suggested that the production of red rust may have been due to slight differences in the flow rate of the air being bubbled through the electrolyte, as this was the only possible variable in the system.

2. PDP Corrosion Rates

Table IV summarizes the corrosion rates obtained by the PDP method as a function of oxygen and chloride concentrations. The corrosion rates were determined by graphically extrapolating the linear regions of the polarization curves, the Tafel regions, to obtain I_{corr} which was then converted

Table IV. Average PDP Corrosion Rates as a Function of Oxygen and Chloride Concentrations

O_2 / Cl^-	0 ppm	5.8 ppm	20 ppm
5 ppt	0.64 mdd	5.94 mdd	14.23 mdd
19 ppt	1.30 mdd	16.54 mdd	51.08 mdd
30 ppt	0.98 mdd	24.90 mdd	48.83 mdd

to a corrosion rate. (See Appendix B for details.) Again, as predicted by the model and measured in the IML and LPM tests, as the oxygen or chloride concentrations were increased, the corrosion rate increased. Also noted with the higher oxygen levels was a significant decrease in the linear regions of the polarization curves. However, the graphical methods still proved adequate as the rates obtained by this method compared very favorably with those obtained by the IML method.

3. PSP Test Results

The PSP test results are summarized in Table V. Due to the applied anodic polarization, the corrosion rates obtained by the PSP method were of course higher than those obtained by other methods. Also, it was noticed that localized corrosion (which will be discussed in more detail later) was a dominant mode of attack in the longer PSP test

runs when oxygen was present in the electrolyte. The rates obtained for the deaerated electrolyte compared favorably with those obtained by the other test methods.

Table V. Average PSP Corrosion Rates as a Function of Oxygen and Chloride Concentrations

Cl^- O_2	0 ppm	5.8 ppm	20 ppm
5 ppt	4.16 mdd	6.72 mdd	65.26mdd
19 ppt	5.55 mdd	17.26 mdd	108.40 mdd
30 ppt	7.81 mdd	23.07 mdd	105.55 mdd

4. Discussion

The results of Tables III, IV, and V show a definite trend of increasing corrosion rates as the oxygen and/or chloride concentrations of the electroyltes are increased. The development of this trend is vividly evident in Figure 15 which is a comparison of the corrosion rates obtained by each test method as a function of oxygen and chloride concentrations. The increase in corrosion rates due to Cl^- concentrations can be directly attributed to the increased conductivity of the electrolyte and the subsequent increase in I_{corr} while the increase in corrosion rates due to the addition of oxygen to the electrolyte changes the polarization of the cell by favoring the cathodic reaction

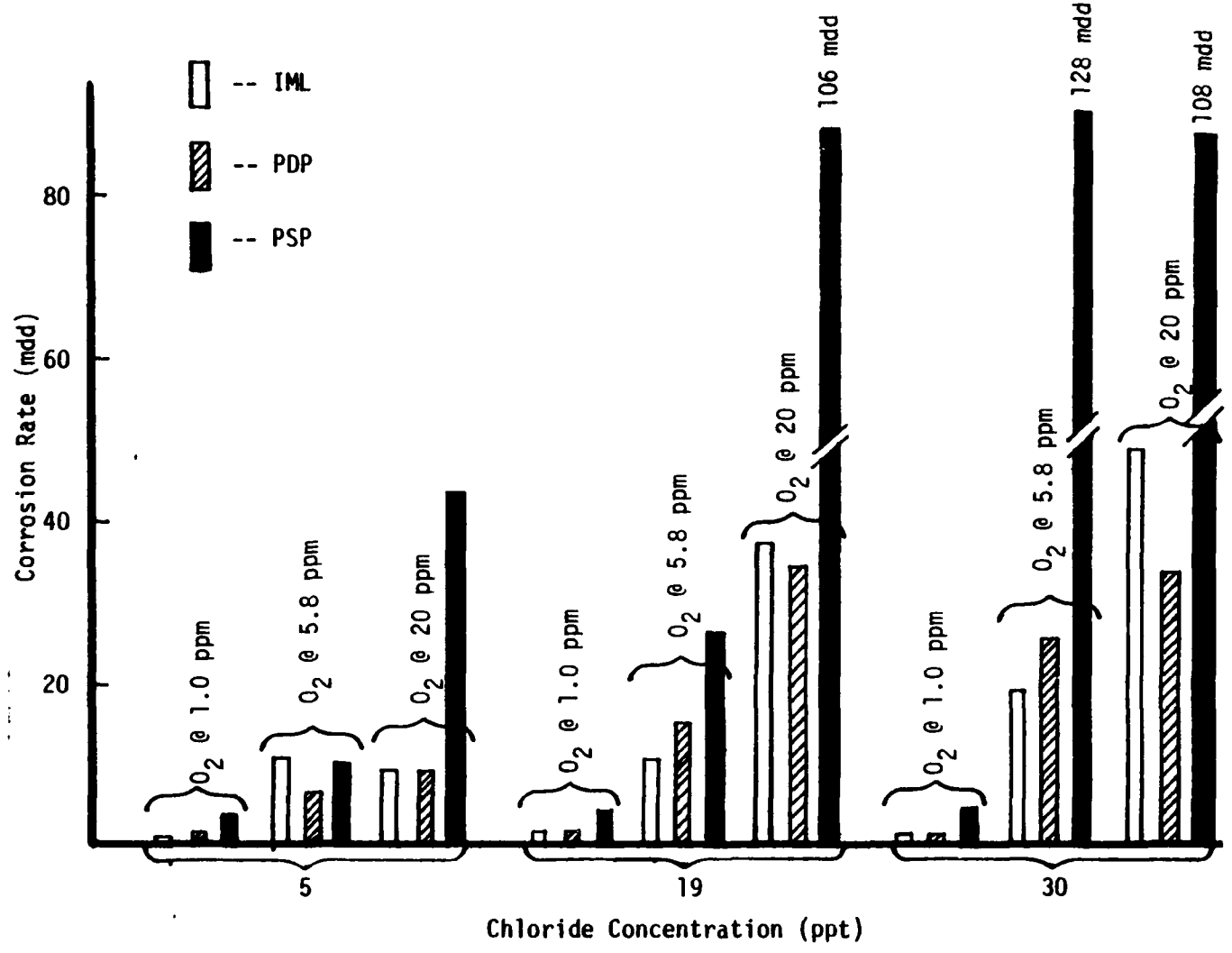

Figure 15. Average Corrosion Rates for 1020 Steel As a Function of Oxygen and Chloride Concentrations for the IML, PDP, and PSP Test Methods.

(Equation 4). While it is realized that a dissolved oxygen level of 20 ppm is not realistically attainable in a natural environment, the dramatic changes in the corrosion rates as a function of oxygen concentration establish a trend which substantiates the results predicted by Equations (4) and (5). This implies that a very effective way to control the corrosion process would be through the elimination of oxygen from the electrolyte.

5. Hierarchy of Corrosion Rate Data

A graphic comparison of the corrosion rates obtained by the IML, PDP, and PSP methods is shown in Figure 15. Overall, the figure shows that the rates obtained by each method compare quite favorably with each other. In establishing a hierarchy or confidence factor for the rates obtained by the various methods, several factors were considered.

(1) How close were the actual measured corrosion rates to the average rates?

(2) How accurate were the measurements used to calculate the corrosion rates?

(3) How did the calculated corrosion rates compare to those obtained by another test method?

(4) How closely did the test simulate the actual environment?

The IML test results would have to be considered the most reliable since the test set-up most closely simulates that found in marine reinforced concrete. Also, the calculated rates were the most consistent as was the ability to make

accurate measurements of the mass loss. The PDP test results were the next most reliable as there was considerably more difficulty encountered in obtaining the values necessary to calculate the corrosion rates. The rates, however, were quite comparable to those obtained by the IML method and were fairly consistent. The PSP test results were the next most reliable. There was little difficulty in making the necessary measurements and calculations, but the rates were somewhat inconsistent due to the tendency for localized corrosion to be the predominant mode of attack in the tests involving aerated electrolytes.

The LPM measurements were not placed in this hierarchy since these are instantaneous rates and generally increased as the IML test progressed. However, the instantaneous rates did remain within a factor of two of the overall corrosion rate for each test, and in the case of the de-aerated electrolyte tests, were very close to those obtained from the IML test. The LPM measurements were perhaps the best indicators of the corrosion process in that they very accurately indicated whether a test coupon was corroding at a steady rate, an increasing rate, or a decreasing rate.

C. DISTRIBUTION AND MODE OF ATTACK

While some general corrosion was seen in most cases, the visually most evident mode of attack in all cases was localized corrosion. Localized attack was obvious at the edges or corners of the test coupons and at the notch formed by

the test coupon and the teflon compression seal of the specimen holder. (See Figure 16.)

Figure 16. Corrosion Product at Notch Formed By Test Coupon and Teflon Compression Seal. (7.65X)

In an attempt to reduce the effect of localized corrosion in the longer (180 and 720 minute) PSP tests, the test coupons were mounted in acrylic plastic to eliminate the notch and edge effects. (See Figure 17.)

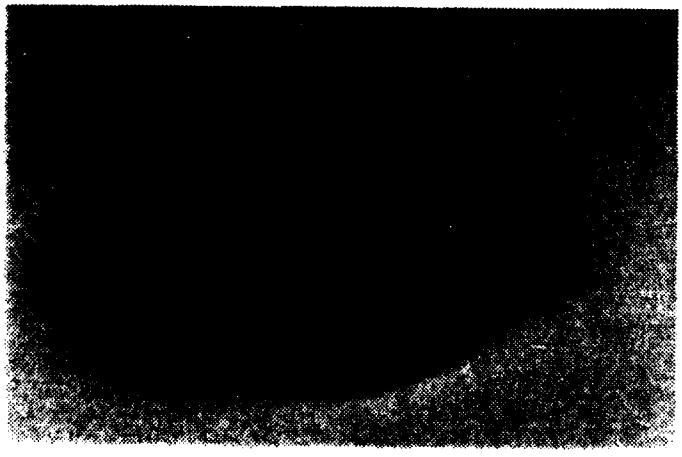

Figure 17. Test Coupon Mounted in Acrylic Plastic.

1. Corrosion Product Distribution

At the completion of each test the test coupons were examined by optical microscopy to determine the effect of oxygen and chloride concentrations on the distribution of corrosion products. It was found that changing the oxygen concentration had no effect on product distribution, but chloride concentration did. Figure 18 shows that as the chloride concentration was increased the distribution of the product became more dense and covered a larger percentage of the surface area. This type of change in product distribution is not unexpected, as it is the Cl^- that breaks down the protective passive film initially formed in the highly alkaline environment. The changes seen in Figures 18 confirm that as the chloride concentration of the electrolyte increases the probability of breaking down the passive film becomes much higher. This leads to more breaks in the protective film and thus the denser product distribution as shown. A similar pattern is seen in SEM micrographs such as presented in Figure 19. Unlike IML test coupons tested in electrolytes of higher and lower oxygen content, the test coupons that produced the surfaces seen in these micrographs were uniformly covered with corrosion product. The corrosion product density in Figure 19 (b), for electrolyte containing 19 ppt Cl^- , seems to be more extensive than that of Figure 19 (a), for electrolyte containing 5 ppt Cl^-. Figure 19 (b) exhibits what appears to be the beginning of an additional layer of corrosion product.

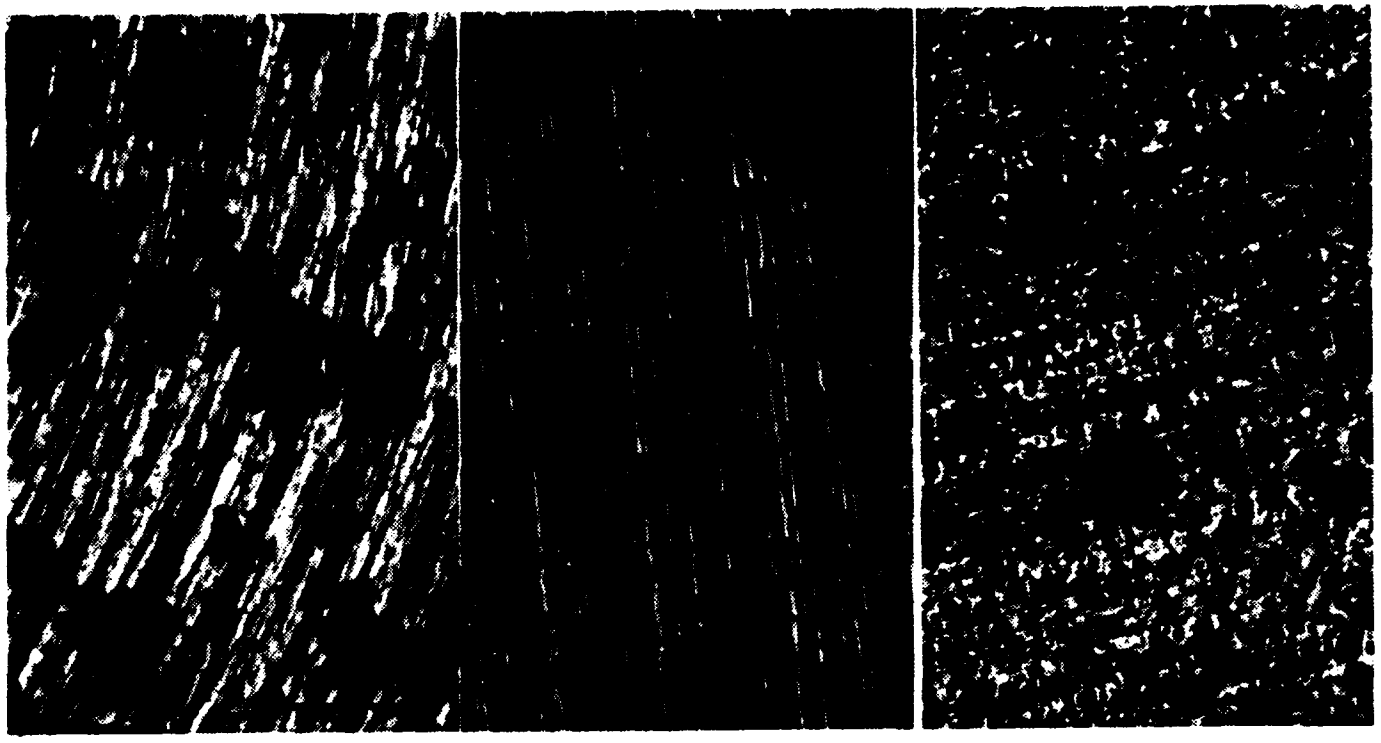

(a) (b) (c)

Figure 18. Optical Micrographs of PDP Test Coupons Showing the Corrosion Product Distribution as a Function of Chloride Concentration. As the Chloride Concentration Increases, from 5 ppt in (a) to 19 ppt in (b) to 30 ppt in (c), the Corrosion Product Becomes Much Finer and More Uniformly Distributed. The Oxygen Concentration Was the Same for Each Case Shown Above, 5.8 ppm. Magnification 400X [(a) 1-C5,PDP (b) 1-C19,PDP (c) 2-C30,PSP]

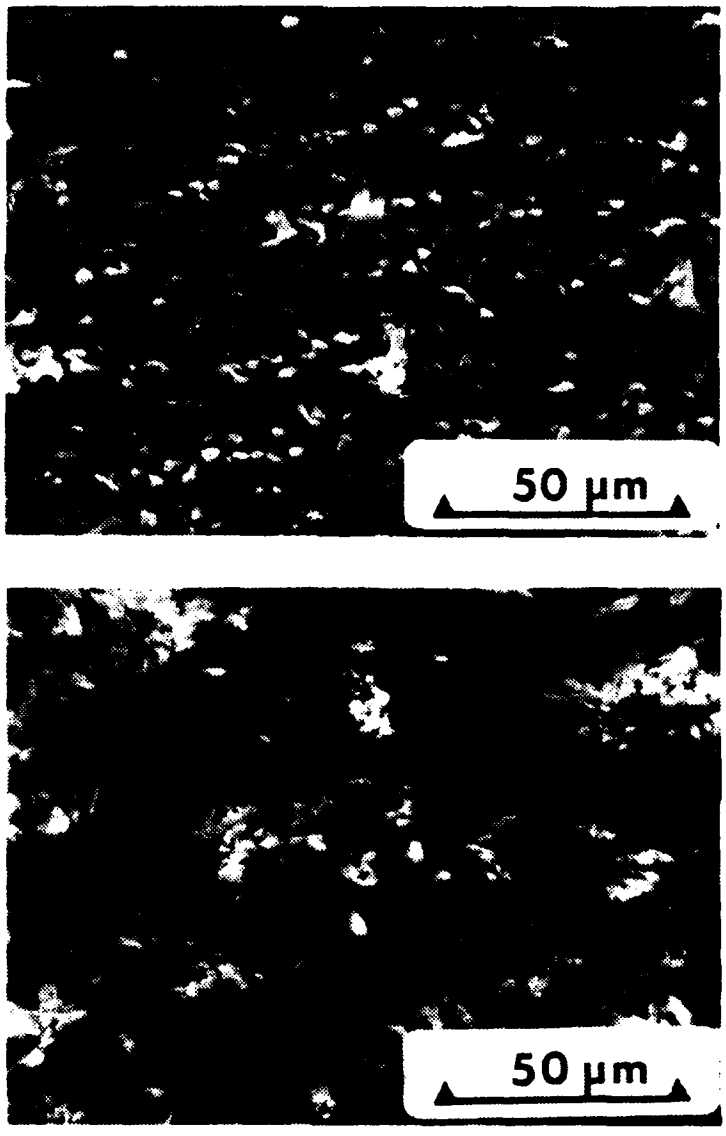

(a)

(b)

Figure 19. SEM Micrographs of IML Test Coupons Showing the Corrosion Product Distribution as a Function of Chloride Concentration. The Micro-Crystalline Form of the Product is Much More Densely Packed in (b) Than in (a) and (b) Appears to Be Forming an Additional Layer of Product. The Chloride Concentration of (a) was 5 ppt and (b) was 19 ppt. The oxygen Concentration for Each Case Was 5.8 ppm. Magnification 650X [(a) 1-C5,IML (b) 1-C19,IML].

Macroscopically, the most prominent corrosion product development was that associated with sites of localized corrosion. Microscopically, one such site is shown in Figure 20. This case is somewhat untypical in that this particular pit formed on a surface away from any notches or corners of the test coupon. However, the form of the product and the build-up of a ridge around the site which was attacked was identical to that seen in all instances of localized attack. The pattern of light and dark areas at the bottom of the pit correspond very closely to the distribution of ferrite and pearlite in the microstructure of 1020 steel. (See Figure E-2 for microstructural comparisons.) These areas very likely correspond to regions of ferrite and pearlite with overlying corrosion product films of somewhat different character. Figure 20 (b) shows the pit after removal of the corrosion product. There are many missing grains in this micrograph and the surface has a faceted appearance indicative of intergranular attack. Localized attack also took the form of microcrystalline growths like that shown in Figure 21. The corrosion product seen here is ferrous hydroxide (red rust).

2. Mode of Attack

As was pointed out earlier, the visually most evident mode of attack is localized corrosion at crevices, notches, or corners of the test coupons. Further investigation of these sites, by scanning electron microscopy, revealed

(a)

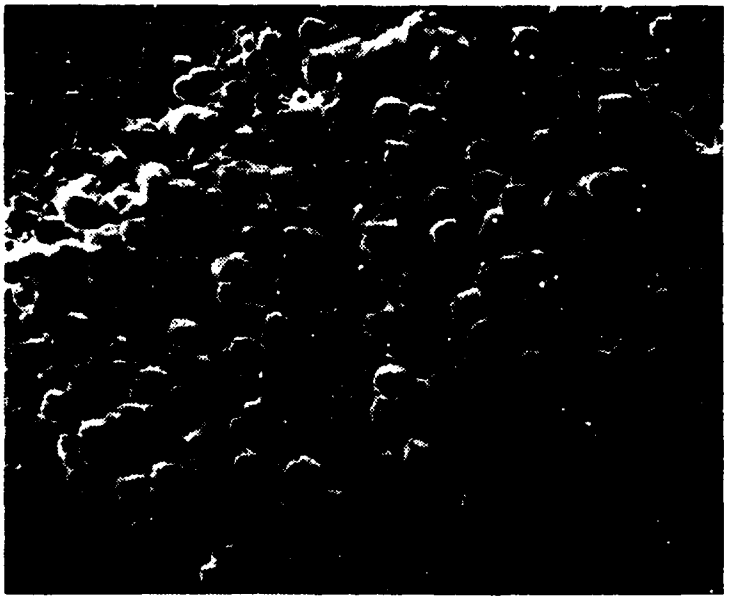

(b)

Figure 20. SEM Micrograph of a Pit on the Surface of an IML Test Coupon, Before and After Corrosion Product Removal. (a) The Pit, Before Removal of the Corrosion Product, Has a Crater-Like Appearance With a Ridge-Like Build-Up of Corrosion Product Around the Central Portion. (b) Removal of the Corrosion Product Reveals Numerous Missing Grains and a Faceted Appearance, Indicative of Intergranular Attack. The Electrolyte Contained 5 ppt Cl^- and was Deaerated. (a) Magnification 300X (b) Magnification 270X [3-A5,IML]

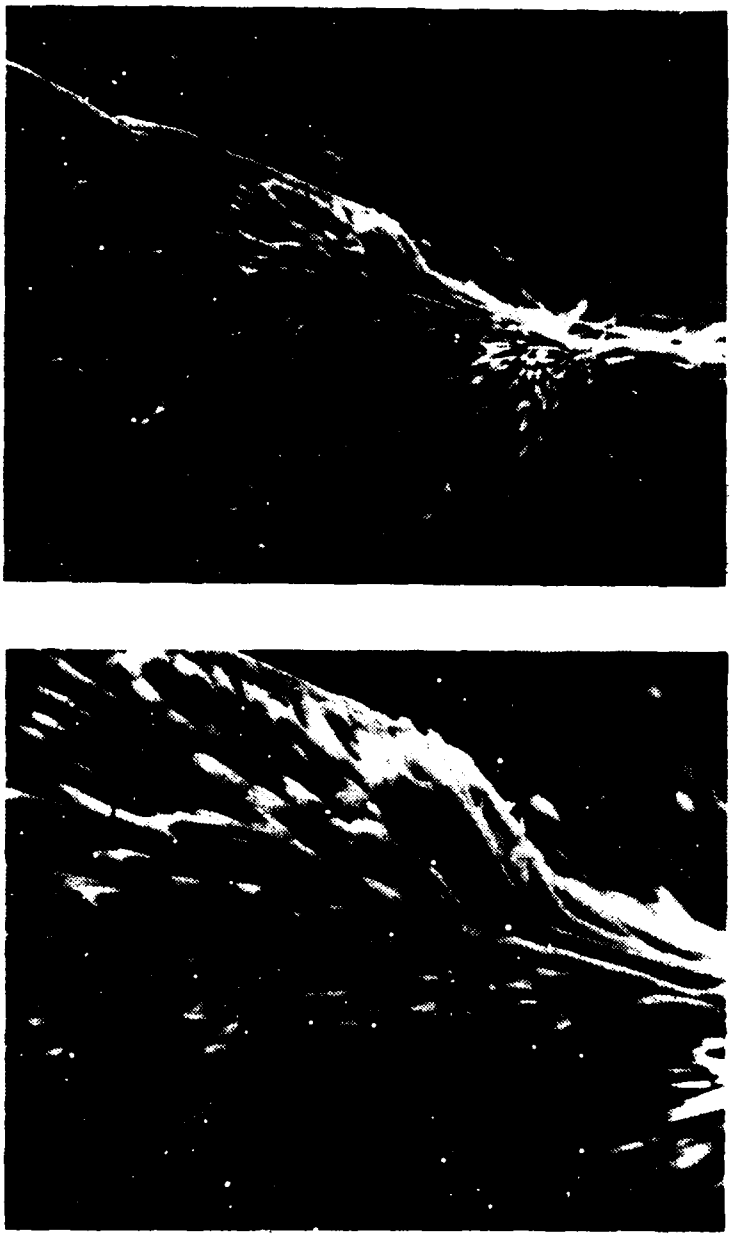

(a)

(b)

Figure 21. SEM Micrograph of PDP Test Coupon. The Attack Seen Here Is a Very Localized Growth of Ferrous Hydroxide (Red Rust). The Electrolyte Contained 30 ppt Cl^- and Was Deaerated. (a) Magnification 270X (b) Magnification 650X [10-A30,PSP]

the features seen in Figures 22 and 23. These figures quite clearly show numerous sites where entire grains are missing, as well as grain boundary intersections and distinct regions of ferrite and pearlite. The smooth faceted appearance of the ferrite grain regions indicates that the corrosion process was intergranular, with little or no effect on the adjacent microstructure.

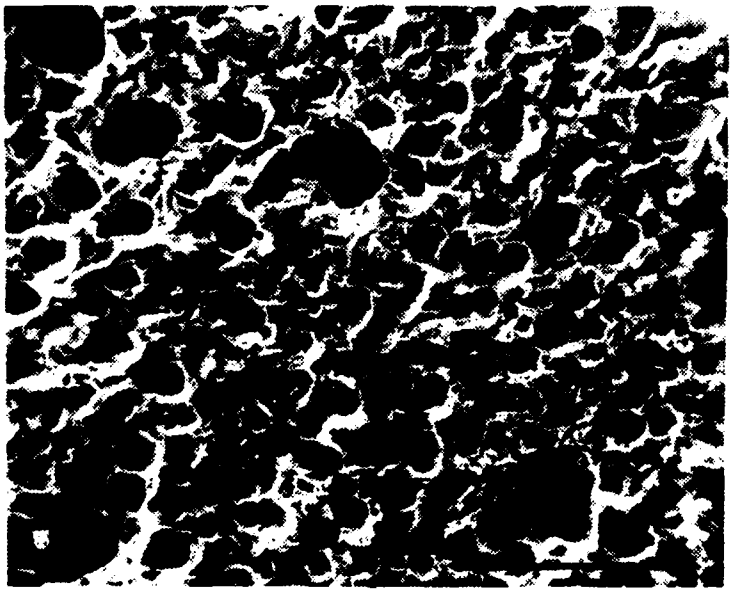

Figure 22. SEM Micrograph of PSP Test Coupon Which Experienced Localized Corrosion. Corrosion Product Was Removed By Ultrasonic Cleaning in Cold Acid for a Few Seconds. There Are Numerous Missing Grains and the Surface Is Faceted, as in Intergranular Corrosion. The Electrolyte Contained 30 ppt Cl^- and Was Deaerated. Magnification 300X [6-A30,PSP]

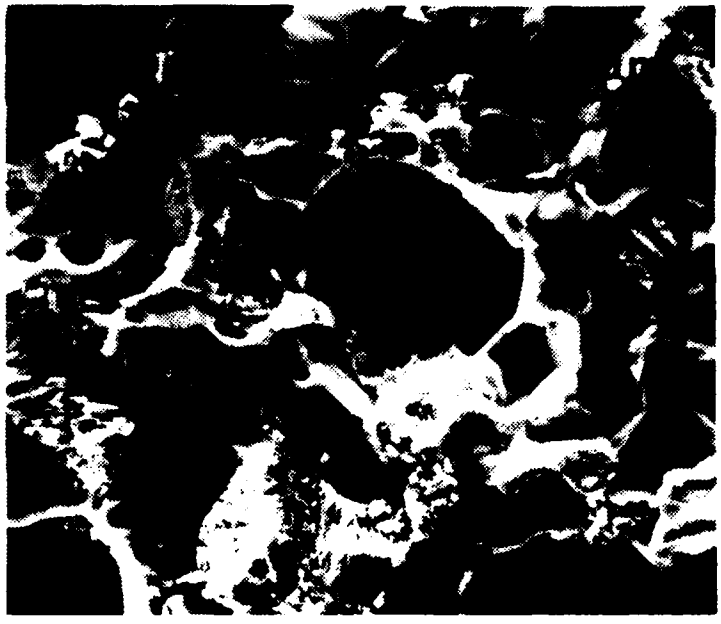

(a)

(b)

Figure 23. SEM Micrographs of PSP Test Coupon in Region of Intergranular Corrosion. The Regions of Ferrite and Pearlite Are Clearly Delineated Here as Well as the Facets of the Remaining Grains. The Electrolyte Contained 30 ppt Cl^- and Was Deaerated. (a) Magnification 1500X (b) Magnification 3000X [6-A30,PSP]

Figure 24 shows the cleaned surface of an IML test coupon that was uniformly covered with red rust. These micrographs reveal an overall lower degree of corrosion than that seen in Figures 22 and 23, which is as expected, since the region of active corrosion was much larger and so reduced the ratio of cathodic area to anodic area. Indications of microstructurally related attack are given by the clearly delineated regions of ferrite and pearlite. The micrographs of Figure 25 are of a surface which was mechanically cleaned rather than chemically and ultrasonically cleaned. This procedure was used to ensure that the standard procedure of ultrasonically cleaning the test coupons in cold acid was not itself inducing corrosive attack. In the lower part of Figure 25 (a) the same faceted appearance seen in Figures 22 and 23 is evident which establishes the validity of the results obtained with the normal cleaning method. Figure 25 (b) shows an area adjacent to the faceted region which appears to be loosely attached and would probably be removed by the ultrasonic cleaning to reveal a faceted surface. Figures 26, 27, and 28 are further examples of intergranular corrosion observed after various test exposures. Based on the SEM results taken as a whole, it would appear that the 1020 steel rebar is attacked preferentially along the ferrite-pearlite boundaries.

(a)

(b)

Figure 24. SEM Micrographs of an IML Test Coupon Surface After Removal of the Corrosion Product Which Had Uniformly Covered the Test Coupon. Microstructural Attack Is Evident From the Clear Delineation of the Regions of Ferrite and Pearlite. The Chloride Concentration of the Electrolyte Was 5 ppt and the O_2 Concentration Was 5.8 ppm. Magnifications (a) 1300X (b) 2600X [2-C5,IML]

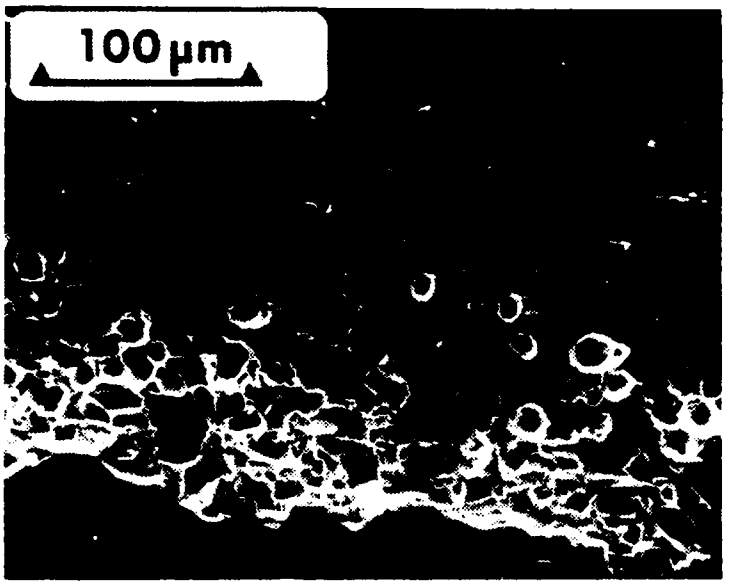

(a)

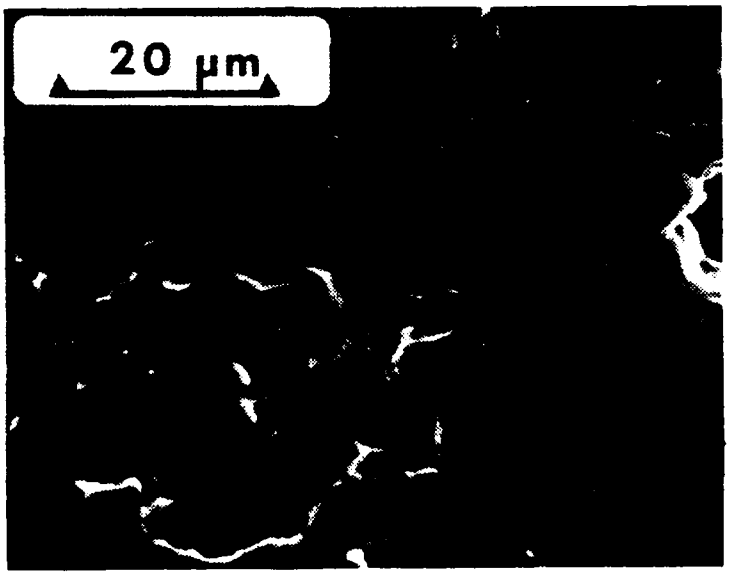

(b)

Figure 25. SEM Micrographs of PSP Test Coupon Surface Which Was Mechanically Cleaned Rather Than Chemically Cleaned and Ultrasonically Cleaned. The Electrolyte Contained 30 ppt Cl^- and 20 ppm O_2. (a) Magnification 290X (b) Magnification 1450X [8-B30,PSP]

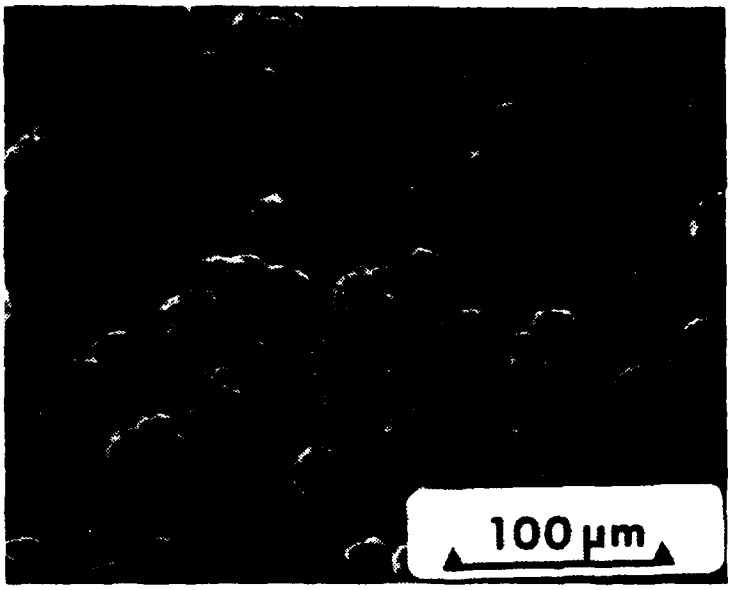

(a)

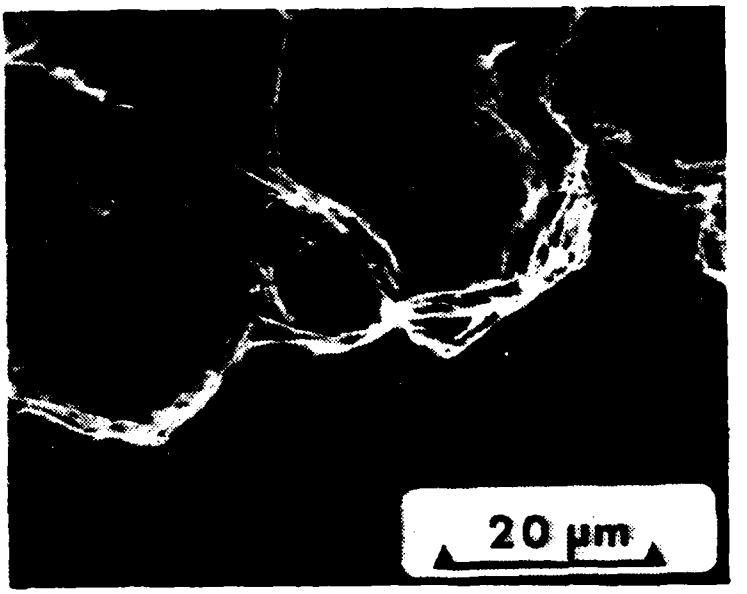

(b)

Figure 26. SEM Micrograph of a PSP Test Coupon Which Has Been Corroded Intergranularly. In (b) the Ferrite and Pearlite Regions Are Clearly Delineated as Are the Smooth Facets of the Ferrite Grains. The Electrolyte Contained 30 ppt Cl^- and Was Deaerated. (a) Magnification 290X (b) Magnification 1450X [10-A30,PSP]

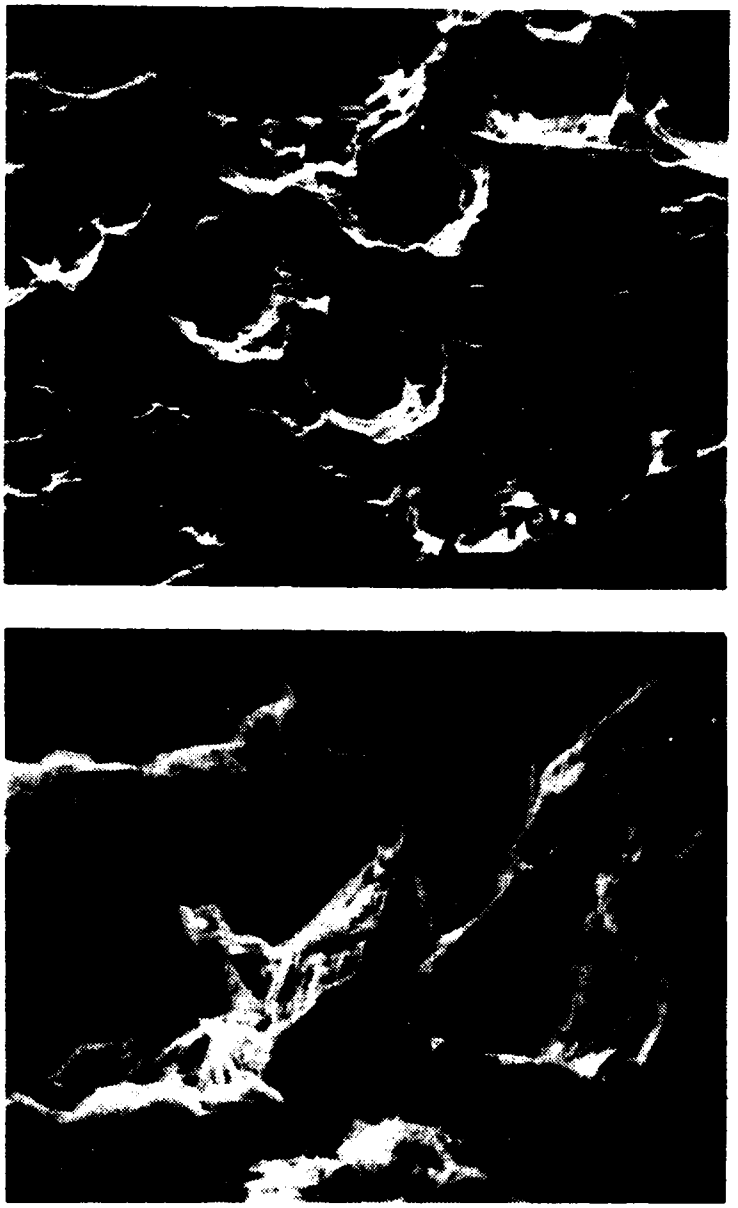

(a)

(b)

Figure 27. SEM Micrographs of an IML Test Coupon Which Has Been Corroded Intergranularly. The Regions of Ferrite and Pearlite Are Clearly Delineated. The Electrolyte Contained 5 ppt Cl^- and 20 ppm O_2. (a) Magnification 630X (b) Magnification 2400X [2-B5,IML]

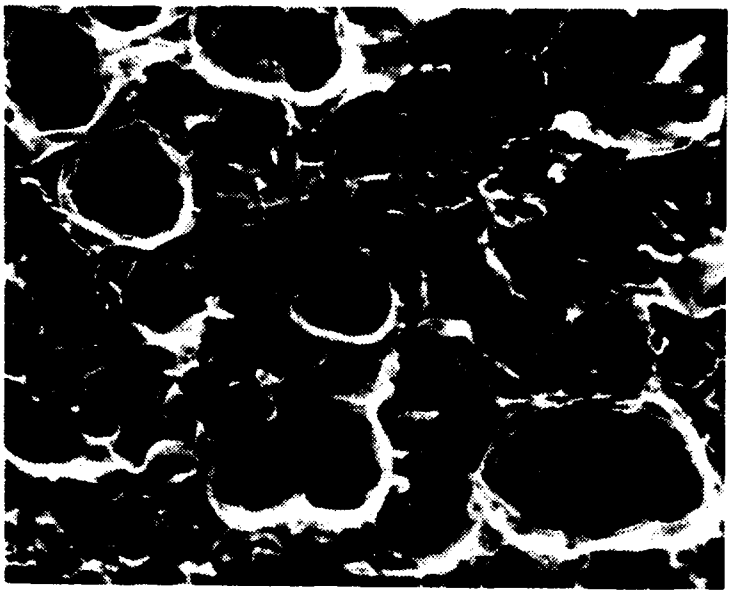

Figure 28. SEM Micrograph of a PSP Test Coupon Which Has Been Corroded Intergranularly. Regions of Ferrite and Pearlite Are Clearly Delineated as Are Numerous Grain Boundaries and Intersections. The Electrolyte Contained 19 ppt Cl^- and 20 ppm O_2. Magnification 720X [8-B19,PSP]

3. Summary of Microscopic Observations

The observations of corrosion product distribution show a strong dependence on the chloride concentration of the electrolyte for general corrosion and a strong tendency to form localized corrosion deposits. This is quite clearly shown in Figures 16 and 18. No change in corrosion product distribution as a function of dissolved oxygen concentrations of the electrolytes was observed.

The SEM studies have clearly shown that the corrosion of 1020 steel in $Ca(OH)_2$ proceeds preferentially along the ferrite-pearlite grain boundaries, as seen in Figure 24

for example. Whether or not this mode of corrosion is significant with respect to rebar in concrete is not clear and would probably require analysis of rebar which has actually been imbedded in concrete.

The corrosion product distribution as a function of chloride content of the electrolyte can be predicted by the observation that as Cl^- content increases, the likelihood of a breakdown of the passive film becomes much greater. On the other hand, neither the literature on imbedded metal corrosion in concrete nor the electrochemical model predict the intergranular mode of corrosion observed during the course of this research.

IV. CONCLUSIONS AND RECOMMENDATIONS

A. CONCLUSIONS

1. The presence of chloride in the electrolyte surrounding the rebar tends to break down the passive film initially formed by the highly alkaline environment, thus lowering the pH locally, and creating a conditions which favors corrosion of the rebar.

2. The addition of oxygen to the electrolyte favors the cathodic reaction in the corrosion cell increasing the potential difference between anode and cathode and increasing I_{corr} which results in an increase in corrosion rate.

3. The absence of oxygen from the electrolyte, as in the deaerated test cells, keeps the corrosion rate at very low values, which is of course desirable in designing structures.

4. The mode of corrosion of 1020 steel in the electrolytes used in the conduct of this research was intergranular.

5. Localized corrosion was a significant form of corrosive attack seen throughout the series of tests implying that crevice situations created adjacent to rebar in reinforced concrete structures could serve as sites of corrosion initiation and localized attack.

B. RECOMMENDATIONS

The problem of imbedded metal corrosion in concrete continues to cause early failure of reinforced concrete structures at a time when the ever-increasing costs of labor and materials demand that a product be useful for its designed service life and often beyond. Continued research to determine methods of eliminating or reducing corrosion of rebar in concrete is vital if designers and manufacturers wish to continue using reinforced concrete in structures like the off-shore oil production platforms of the North Sea or other sea structures that could cause environmental damage in the event of early failure due to corrosion of rebar. Some of the issues which have been and should continue to be addressed by researchers are listed below.

1. The introduction of chlorides to concrete in aggregates, mixing water, admixtures, and curing agents (such as $CaCl_2$).
2. The use of inhibitors to reduce or eliminate corrosion.
3. The use of different alloys as rebar.
4. The use of cathodic protection in new and reconstructed structures.
5. The use of metallic and chemical coatings on rebar.

APPENDIX A: BASIC CORROSION TERMINOLOGY AND DEFINITIONS

Admixture -- a material other than water, aggregates, and hydraulic cement, used as an ingredient of concrete or mortar, and added to the batch immediately before or during its mixing. It acts as an air entrainer, curing accelerator or retarder, or a water reducer.

Aggregate -- a mixture of sand and gravel which is mixed with cement to form concrete.

Buffer -- a substance, or mixture of substances, which when present in an electrolytic solution tends to diminish fluctuations of pH.

Carbonation -- the impregnation of a substance or solution with carbon dioxide.

Corrosion Potential -- the potential resulting from the mutual polarization of the interfacial potentials of the partial anodic and cathodic reactions that constitute the overall corrosion reaction.

Corrosion Product -- metal reaction product resulting from a corrosion reaction; solid, liquid, or gas (eg., $2\ Fe + 2\ H_2O + O_2 \rightarrow 2\ Fe(OH)_2$).

Crevice Corrosion -- localized corrosion resulting from a crevice formed between two surfaces - one at least of which is a metal.

Electrolyte -- a substance which in solution contains ions.

Fouling -- the attachment and growth of marine organisms on a submerged surface.

Intergranular Corrosion -- preferential corrosion which proceeds along grain boundaries.

pH -- a measure of the hydrogen ion activity defined by the relation $pH = -\log a_{H^+}$; where a_{H^+} is the activity of the hydrogen ion.

Spalling -- the break-up of a surface through the operation of internal expansive forces.

APPENDIX B: REPRESENTATIVE CALCULATIONS FOR CORROSION RATES

Corrosion rates were calculated from measured data and recorded as a penetration rate (mils per year, mpy) and as a mass loss rate (milligrams per square decimeter per day, mdd).

$$RATE_{penetration} = \frac{A\, i_{corr}}{z\, F\, \rho} \qquad (B - 1)$$

$$RATE_{mass\ loss} = \frac{A\, i_{corr}}{z\, F} \qquad (B - 2)$$

$F = 9.64848 \times 10^4$ coulombs/equivalent, Faraday's Constant

$\rho = 7.859$ grams/cm^3 , density of 1020 Steel

i_{corr} = current density in amps/cm^2

A = Atomic weight, 55.734 grams/cm^3 for 1020 Steel

z = valence equivalents/mole , 2 used in all calculations

<u>For IML Tests</u>

$$RATE_{mass\ loss} = \frac{\text{(measured weight loss in mg)}}{\text{(area in dm) (time of test in days)}} \qquad (B - 3)$$

then $= R_{mdd}$

$$RATE_{penetration} = \frac{R_{mdd} \times 1.437}{\rho} = R_{mpy} \qquad (B - 4)$$

For PSP Tests

The area under the current vs time curve is used to determine the mass loss during the period of the test and is calculated by applying Faraday's Law:

$$\text{mass lost} = A/zF \int I\, dt$$

where $\int I\, dt$ is the area under the curve. The area under the curve was calculated using Simpson's approximation and a programmable calculator. The calculated mass loss is then converted to rates by using equations B-3 and B-4.

For PDP Tests

I_{corr} is measured directly from the PDP curves as shown in Figure B-1. This is converted to a current density by dividing by the surface area of the test coupon and then using Equations B-1 and B-2.

For LPM Tests

The polarization resistance, $\frac{\Delta E}{\Delta I}$, is measured from the Linear Polarization Plots and substituted into the Stearn-Geary equation:

$$I_{corr} = \frac{\beta_a \beta_c}{2.3\ (\beta_a \beta_c)} \quad \frac{\Delta I}{\Delta E}$$

β = Tafel constant as determined from the PDP curves

$$i_{corr} = \frac{I_{corr}}{\text{Surface area}}$$

then substituting into equations B-1 and B-2 gives the corrosion rates.

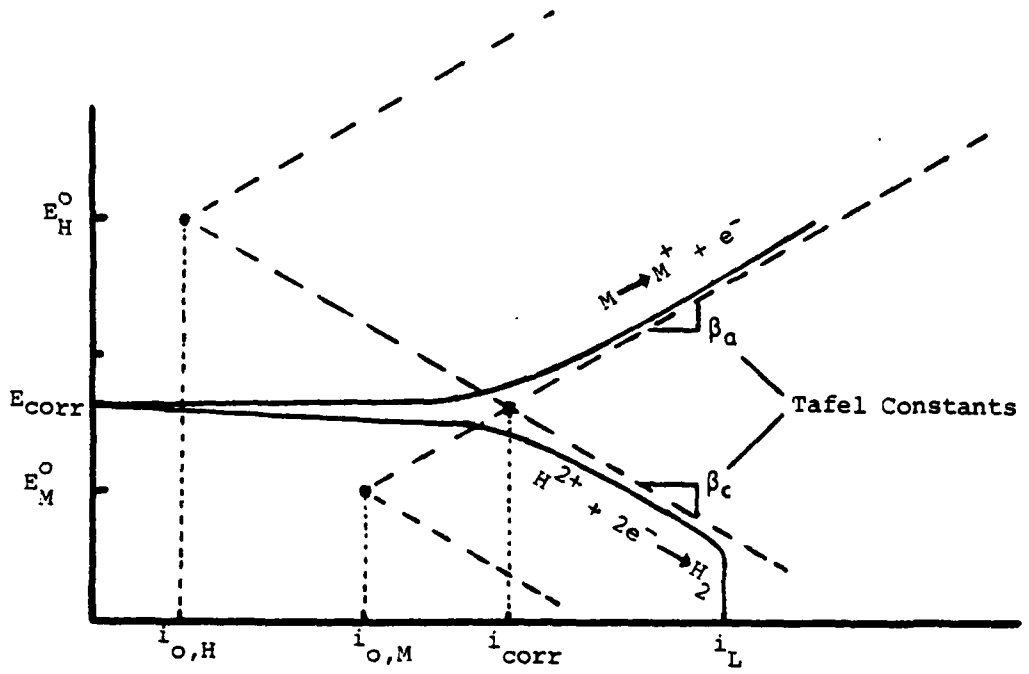

Figure B-1. Schematic Representation of Potentiodynamic Polarization Curve

APPENDIX C: REPRESENTATIVE CALCULATIONS AND PROCEDURES FOR ELECTROLYTE PREPARATION

The electrolyte for this study was based on a saturated calcium hydroxide ($Ca(OH)_2$) solution which represents the ideal environment in concrete. The effect of varying Cl^- and dissolved O_2 concentrations and of varying the pH of the electrolyte were examined.

In preparing the electrolyte, a solution containing the desired Cl^- concentration was first obtained. Calcium chloride, dihydrate, $CaCl_2 \cdot 2H_2O$, was used to prepare the solution in the following manner:

Molecular weight $CaCl_2 \cdot 2H_2O$ = 147.018 g/mole

→ fraction Cl^- = 48.229 %

to obtain the desired concentration in parts per thousand (ppt), the volume of H_2O is found as follows:

$$\frac{\text{Desired } [Cl^-] \text{ g}}{1000 \text{ ml } (H_2O)} = \frac{(\text{Measured weight of } CaCl_2 \cdot 2H_2O) \text{ g} \times 0.48229}{(\text{Volume } H_2O \text{ needed}) \text{ ml}}$$

$$\rightarrow (\text{Volume } H_2O \text{ needed}) \text{ ml} = \frac{(\text{Meas wt } CaCl_2 \cdot 2H_2O) \times (0.48229) \times (1000)}{\text{Desired } Cl^- \text{ concentration}}$$

Once the solution with the desired chloride concentration was obtained, calcium hydroxide was added to saturate the solution, usually about 2.0 grams/liter. The solubility limit for calcium hydroxide in water at 25°C is 1.85 grams

per liter. The excess calcium hydroxide was used to allow for the formation of calcium carbonate, $CaCO_3$, and to provide a reserve of calcium hydroxide in solution to ensure that it remained saturated.

APPENDIX D: TEST DATA

Tables D-I through D-IV-L contain the data collected from the various tests. The following notes describe recurring parameters in each of the tables.

Note 1: The average dissolved oxygen content for Series A tests was 1.06 ppm.

Note 2: The average dissolved oxygen content for Series B tests was 20.0 ppm.

Note 3: The average dissolved oxygen content for Series C tests was 5.73 ppm.

Note 4: The average pH of electrolytes containing 5 ppt Cl^- was 12.38.

Note 5: The average pH of electrolytes containing 19 ppt Cl^- was 12.19.

Note 6: The average pH of electrolytes containing 30 ppt Cl^- was 12.01.

IML DATA

TABLE D-I

IMMERSION MASS LOSS TEST RESULTS

		SERIES A			SERIES C			SERIES B		
Specimen #	Cl^- (ppt)	Mass Loss (mg)	R_{mdd}	R_{mpy}	Mass Loss (mg)	R_{mdd}	R_{mpy}	Mass Loss (mg)	R_{mdd}	R_{mpy}
1		0.6	0.43	0.08	15.4	11.40	2.09	21.4	15.64	2.86
2	5	0.9	0.65	0.12	25.2	18.98	3.48	24.6	18.22	3.33
3		1.1	0.81	0.15	19.7	14.71	2.69	13.0	9.44	1.73
1		1.8	1.31	0.24	15.2	11.45	2.09	88.0	66.64	12.18
2	19	1.3	0.97	0.18	15.3	11.28	2.06	63.4	49.10	8.98
3		1.6	1.19	0.22	16.0	11.56	2.11	55.1	39.80	7.28
1		2.2	1.99	0.37	24.5	18.24	3.34	88.8	64.32	11.76
2	30	1.9	1.37	0.25	21.7	16.43	3.00	105.3	80.74	14.76
3		1.3	0.95	0.17	29.7	22.43	4.10	102.2	76.57	14.00

LPM DATA

TABLE D-II A

LINEAR POLARIZATION TEST RESULTS
CHLORIDE CONCENTRATION @ 5 ppt

Specimen #	Elapsed Time (hrs)	SERIES A E_{CORR} vs SCE	SERIES A R_{mdd}	SERIES A R_{mpy}	SERIES C E_{CORR} vs SCE	SERIES C R_{mdd}	SERIES C R_{mpy}	SERIES B E_{CORR} vs SCE	SERIES B R_{mdd}	SERIES B R_{mpy}
	6	-.371	2.05	0.37	-.354	5.10	0.93	-.375	33.53	6.13
	108	-.159	0.35	0.06	-.459	23.36	4.27	-.449	44.01	8.05
	192	-.302	0.47	0.09	-.467	23.36	4.27	-.445	35.62	6.51
	289	-.090	1.17	0.21	-.454	23.36	4.27	-.449	35.62	6.51
1	390	-.178	1.06	0.19	-.499	19.11	3.49	-.464	39.82	7.28
	492	-.166	1.17	0.21	-.479	17.42	3.18	-.429	35.62	6.51
	576	-.116	1.11	0.20	-.575	57.34	10.48	-.458	48.20	8.81
	671	-.206	1.19	0.22	-.666	67.96	12.43	-.434	44.01	8.05
	6	-.539	2.06	0.38	-.285	3.24	0.59	-.447	53.09	9.71
	108	-.386	0.23	0.04	-.455	25.92	4.74	-.450	50.35	7.38
	192	-.300	0.52	0.09	-.446	19.44	3.55	-.447	38.23	6.99
	289	-.141	0.43	0.08	-.453	21.60	3.96	-.464	46.72	8.54
2	390	-.224	0.35	0.06	-.529	19.44	3.55	-.492	50.97	9.32
	492	-.224	0.29	0.05	-.506	15.12	2.76	-.439	44.60	8.15
	576	-.201	0.37	0.07	-.665	129.58	23.69	-.464	44.60	8.15
	671	-.350	0.39	0.07	-.691	129.58	23.69	-.456	44.60	8.15
	6	-.544	1.68	0.31	-.385	9.43	1.72	-.425	35.46	6.48
	108	-.370	1.12	0.20	-.454	23.56	4.31	-.424	31.25	5.71
	192	-.200	1.52	0.28	-.482	23.56	4.31	-.434	39.58	7.24
	289	-.148	0.38	0.07	-.460	23.56	4.31	-.428	31.25	5.71
3	390	-.252	0.27	0.05	-.528	17.14	3.13	-.454	29.16	5.33
	492	-.371	0.42	0.08	-.696	12.42	2.27	-.399	22.92	4.19
	576	-.472	1.09	0.20	-.690	113.53	20.76	-.411	20.83	3.81
	671	-.556	1.12	0.20	-.702	113.53	20.76	-.398	16.67	3.05

TABLE D-II B

LINEAR POLARIZATION TEST RESULTS (CONT'D)
CHLORIDE CONCENTRATION @ 19 ppt

Specimen #	Elapsed Time (hrs)	SERIES A E_{CORR} vs SCE	SERIES A R_{mdd}	SERIES A R_{mpy}	SERIES C E_{CORR} vs SCE	SERIES C R_{mdd}	SERIES C R_{mpy}	SERIES B E_{CORR} vs SCE	SERIES B R_{mdd}	SERIES B R_{mpy}
	6	-.610	2.10	0.38	-.448	37.29	6.82	-.442	73.85	13.50
	108	-.475	0.42	0.08	-.460	22.79	4.17	-.473	84.71	15.49
	192	-.541	0.34	0.06	-.464	20.72	3.79	-.495	95.57	17.47
	289	-.370	0.65	0.12	-.509	20.72	3.79	-.488	117.29	21.44
1	390	-.532	0.61	0.11	-.573	24.86	4.55	-.481	162.90	29.78
	492	-.524	0.61	0.11	-.545	26.93	4.92	-.487	167.24	30.58
	576	-.471	0.74	0.14	-.554	29.01	5.30	-.497	186.79	34.15
	671	-.405	1.35	0.25	-.586	35.22	6.44	-.518	182.45	33.36
	6	-.589	1.71	0.31	-.442	40.17	7.34	-.463	73.29	13.40
	108	-.410	0.63	0.11	-.464	23.26	4.25	-.489	91.06	16.65
	192	-.456	0.64	0.12	-.472	23.26	4.25	-.507	108.83	19.90
	289	-.297	1.00	0.18	-.466	21.14	3.87	-.476	93.28	17.05
2	390	-.421	0.23	0.04	-.558	21.14	3.87	-.474	97.72	17.87
	492	-.429	0.53	0.10	-.526	23.26	4.25	-.457	99.94	18.27
	576	-.428	0.49	0.08	-.548	48.63	8.89	-.467	86.62	15.84
	671	-.438	0.49	0.09	-.600	57.08	10.44	-.473	86.62	15.84
	6	-.490	1.28	0.23	-.444	39.31	7.19	-.460	70.44	12.88
	108	-.324	1.06	0.19	-.478	23.76	4.34	-.471	66.30	12.12
	192	-.352	0.43	0.08	-.468	28.08	5.13	-.474	60.08	10.98
	289	-.207	0.19	0.04	-.464	43.19	7.90	-.446	47.65	8.71
3	390	-.368	0.09	0.02	-.588	34.55	6.32	-.430	45.58	7.95
	492	-.352	0.15	0.03	-.580	41.03	7.50	-.406	43.51	7.95
	576	-.344	0.09	0.02	-.601	51.83	9.48	-.470	105.66	19.32
	671	-.308	0.13	0.02	-.600	62.63	11.45	-.499	155.39	28.41

TABLE D-II C

LINEAR POLARIZATION TEST RESULTS (CONT'D)
CHLORIDE CONCENTRATION @ 30 ppt

Specimen #	Elapsed Time (hrs)	SERIES A E_{CORR} vs SCE	SERIES A R_{mdd}	SERIES A R_{mpy}	SERIES C E_{CORR} vs SCE	SERIES C R_{mdd}	SERIES C R_{mpy}	SERIES C E_{CORR} vs SCE	SERIES C R_{mdd}	SERIES C R_{mpy}
	6	-.548	25.06	4.58	-.456	23.82	4.36	-.504	95.55	17.47
	108	-.532	2.55	0.47	-.460	41.15	7.52	-.524	143.33	26.20
	192	-.429	27.82	5.09	-.432	49.81	9.11	-.480	122.56	22.41
	289	-.391	4.46	0.82	-.512	47.64	8.71	-.464	101.79	18.61
1	390	-.529	4.04	0.74	-.539	34.65	6.34	-.484	101.79	18.61
	492	-.504	4.46	0.82	-.571	36.81	6.73	-.479	132.95	24.31
	576	-.470	4.04	0.74	-.562	56.30	10.29	-.487	176.57	32.28
	671	-.450	3.19	0.58	-.593	69.30	12.67	-.498	193.19	35.32
	6	-.549	6.22	1.14	-.479	28.24	5.16	-.495	63.77	11.66
	108	-.426	1.87	0.34	-.477	28.24	5.16	-.525	134.14	24.52
	192	-.509	1.87	0.34	-.491	39.10	7.15	-.491	160.53	29.35
	289	-.407	5.59	1.02	-.520	43.44	7.94	-.465	125.34	22.92
2	390	-.417	1.04	0.19	-.617	28.24	5.16	-.491	134.14	24.52
	492	-.425	2.07	0.38	-.625	29.97	5.48	-.479	173.72	31.76
	576	-.433	1.24	0.23	-.607	43.44	7.94	-.480	191.31	34.98
	671	-.441	1.45	0.27	-.601	45.61	8.34	-.496	226.50	41.41
	6	-.508	5.02	0.92	-.464	36.23	6.62	-.512	96.69	17.68
	108	-.373	0.63	0.12	-.500	25.63	4.69	-.532	135.37	24.75
	192	-.588	0.42	0.08	-.500	23.49	4.30	-.472	128.92	23.57
	289	-.305	5.85	1.07	-.535	44.85	8.20	-.448	100.99	18.46
3	390	-.327	4.37	0.80	-.596	32.04	5.86	-.478	107.44	19.64
	492	-.380	3.97	0.73	-.604	42.72	7.81	-.452	100.99	18.46
	576	-.453	1.04	0.19	-.594	57.67	10.54	-.446	100.99	18.46
	671	-.343	1.25	0.23	-.596	74.75	13.67	-.450	100.99	18.46

PDP DATA

TABLE D-III

POTENTIODYNAMIC POLARIZATION TEST RESULTS

Specimen #	Cl^- (ppt)	SERIES A E_{CORR} vs SCE	SERIES A R_{mdd}	SERIES A R_{mpy}	SERIES C E_{CORR} vs SCE	SERIES C R_{mdd}	SERIES C R_{mpy}	SERIES B E_{CORR} vs SCE	SERIES B R_{mdd}	SERIES B R_{mpy}
1		-.436	0.59	0.11	-.440	7.40	1.35	-.335	8.55	1.56
2		-.488	1.20	0.22	-.418	4.25	0.78	-.307	19.84	3.63
3	5	-.422	1.32	0.24	-.434	6.16	1.13	-.358	14.29	2.61
1		-.515	0.99	0.18	-.458	11.34	2.07	-.402	49.60	9.07
2		-.504	1.39	0.25	-.424	27.74	5.07	-.413	48.98	8.95
3	19	-.524	1.53	0.28	-.390	10.54	1.93	-.417	54.67	9.99
1		-.548	1.03	0.19	-.472	22.30	4.08	-.491	52.09	9.52
2		-.551	0.50	0.09	-.465	30.82	5.64	-.492	53.02	9.69
3	30	-.555	1.41	0.26	-.474	21.58	3.94	-.456	41.38	7.57

PSP DATA

TABLE D-IV A

POTENTIOSTATIC POLARIZATION TEST RESULTS
CHLORIDE CONCENTRATION @ 5 ppt

		SERIES A				SERIES C				SERIES B			
Specimen #	Run-Time (min)	E_{CORR} vs SCE	Mass Loss (µg)	R_{mdd}	R_{mpy}	E_{CORR} vs SCE	Mass Loss (µg)	R_{mdd}	R_{mpy}	E_{CORR} vs SCE	Mass Loss (µg)	R_{mdd}	R_{mpy}
1	12	-.605	0.96	2.35	0.43	-.331	0.58	5.68	1.04	-.350	13.46	35.03	6.40
2	12	-.554	0.90	2.27	0.42	-.380	0.27	3.31	0.61	-.355	38.52	95.83	17.52
3	12	-.560	0.49	1.22	0.22	-.522	0.71	6.98	1.28	-.387	19.80	49.54	9.06
4	60	-.464	11.54	5.81	1.06	-.339	34.09	68.92	12.60	-.366	182.58	90.13	16.48
5	60	-.585	3.43	1.74	0.32	-.277	5.17	10.11	1.85	-.342	88.45	45.00	8.23
6	60	-.433	21.59	10.87	1.99	-.285	1.10	2.29	0.42	-.373	149.96	76.04	13.90
7	180	-.462	51.27	8.46	1.55	-.268	6.08	3.97	0.73	--	--	--	--
8	180	-.499	22.30	3.72	0.68	-.284	17.51	11.80	2.16	--	--	--	--
9	720	-.471	22.87	0.95	0.17	-.363	35.53	9.62	1.76	--	--	--	--

TABLE D-IV B

POTENTIOSTATIC POLARIZATION TEST RESULTS (CONT'D)
CHLORIDE CONCENTRATION @ 19 ppt

		SERIES A				SERIES C				SERIES B			
Specimen #	Run-Time (min)	E_{CORR} vs SCE	Mass Loss (µg)	R_{mdd}	R_{mpy}	E_{CORR} vs SCE	Mass Loss (µg)	R_{mdd}	R_{mpy}	E_{CORR} vs SCE	Mass Loss (µg)	R_{mdd}	R_{mpy}
1	12	-.576	1.85	4.65	0.85	-.422	2.06	20.86	3.81	-.422	33.35	84.19	15.39
2	12	-.530	2.98	7.48	1.37	-.425	1.85	18.10	3.31	-.447	37.96	94.58	17.29
3	12	-.548	1.81	4.61	0.84	-.451	2.89	29.21	5.34	-.419	35.14	86.26	15.77
4	60	-.570	2.57	1.32	0.24	-.403	9.34	18.88	3.45	-.440	247.03	127.97	23.40
5	60	-.531	7.03	3.50	0.64	-.405	24.15	48.83	8.93	-.442	275.13	139.13	25.44
6	60	-.530	16.17	8.06	1.47	-.412	64.61	130.64	23.88	-.456	157.36	78.02	14.26
7	180	-.548	38.22	6.44	1.18	-.425	453.80	176.69	32.20	--	--	--	--
8	180	-.556	32.99	5.42	0.99	-.459	378.99	39.06	7.14				
9	720	-.520	198.59	8.47	1.55	--	--	--	--	--	--	--	--

TABLE D-IV C

POTENTIOSTATIC POLARIZATION TEST RESULTS (CONT'D)
CHLORIDE CONCENTRATION @ 30 ppt

		SERIES A				SERIES C				SERIES B			
Specimen #	Run-Time (min)	E_{CORR} vs SCE	Mass Loss (µg)	R_{mdd}	R_{mpy}	E_{CORR} vs SCE	Mass Loss (µg)	R_{mdd}	R_{mpy}	E_{CORR} vs SCE	Mass Loss (µg)	R_{mdd}	R_{mpy}
1	12	-.550	2.56	6.46	1.18	-.472	3.24	32.97	5.99	-.454	35.14	86.26	15.77
2	12	-.504	2.03	5.08	0.93	-.444	1.83	17.90	3.27	-.414	46.13	112.91	20.64
3	12	-.532	2.94	7.39	1.35	-.444	141.64	18.52	3.39	-.457	38.46	97.43	17.81
4	60	-.550	9.47	4.64	0.85	-.494	287.00	71.93	13.15	-.431	127.19	72.62	13.28
5	60	-.560	19.88	9.71	1.77	-.495	287.44	144.62	26.44	-.478	369.61	193.77	35.42
6	60	-.569	19.47	9.56	1.75	-.518		146.65	26.81	-.454	139.66	20.30	12.85
7	180	-.576	44.09	7.40	1.35	--	--	--	--	--	--	--	--
8	180	-.570	49.19	8.29	1.52	--	--	--	--	--	--	--	--
9	180	-.552	387.17	16.24	2.97	--	--	--	--	--	--	--	--

APPENDIX E: PHYSICAL/CHEMICAL REFERENCE DATA

I. ELECTROCHEMICAL TABLES AND REFERENCE DIAGRAMS

Table E-I is an abbreviated EMF Series showing the relative positions of some of the reactions of interest in the corrosion process involving steel in concrete.

TABLE E-I - EMF Series [44]

Reduction Reactions	Standard Reduction Potentials (V vs SHE)
$Ca(OH)_2 + 2e^- = Ca^{++} + 2OH^-$	-3.02
$Ca^{++} + 2e^- = Ca$	-2.76
$2H_2O + 2e^- = H_2 + 2OH^-$	-0.8277
Saturated Calomel Electrode	0.2415
$O_2 + 2H_2O + 4e^- = 4OH^-$	0.401
$Fe^{++} + 2e^- = Fe$	0.440
$O_2 + 4H^+ + 4e^- = 2H_2O$	1.229

Table E-II is an abbreviated Galvanic Series, in seawater, showing the relative positions of other alloys which may be considered for use as rebar. Figure E-1 is the Pourbaix diagram for iron. The shaded area indicates the region of

AD-A114 468 NAVAL POSTGRADUATE SCHOOL MONTEREY CA F/G 7/4
AN ELECTROCHEMICAL INVESTIGATION OF CORROSION RATES FOR 1020 ST--ETC(U)
JUN 81 D R SCOTT

UNCLASSIFIED NL

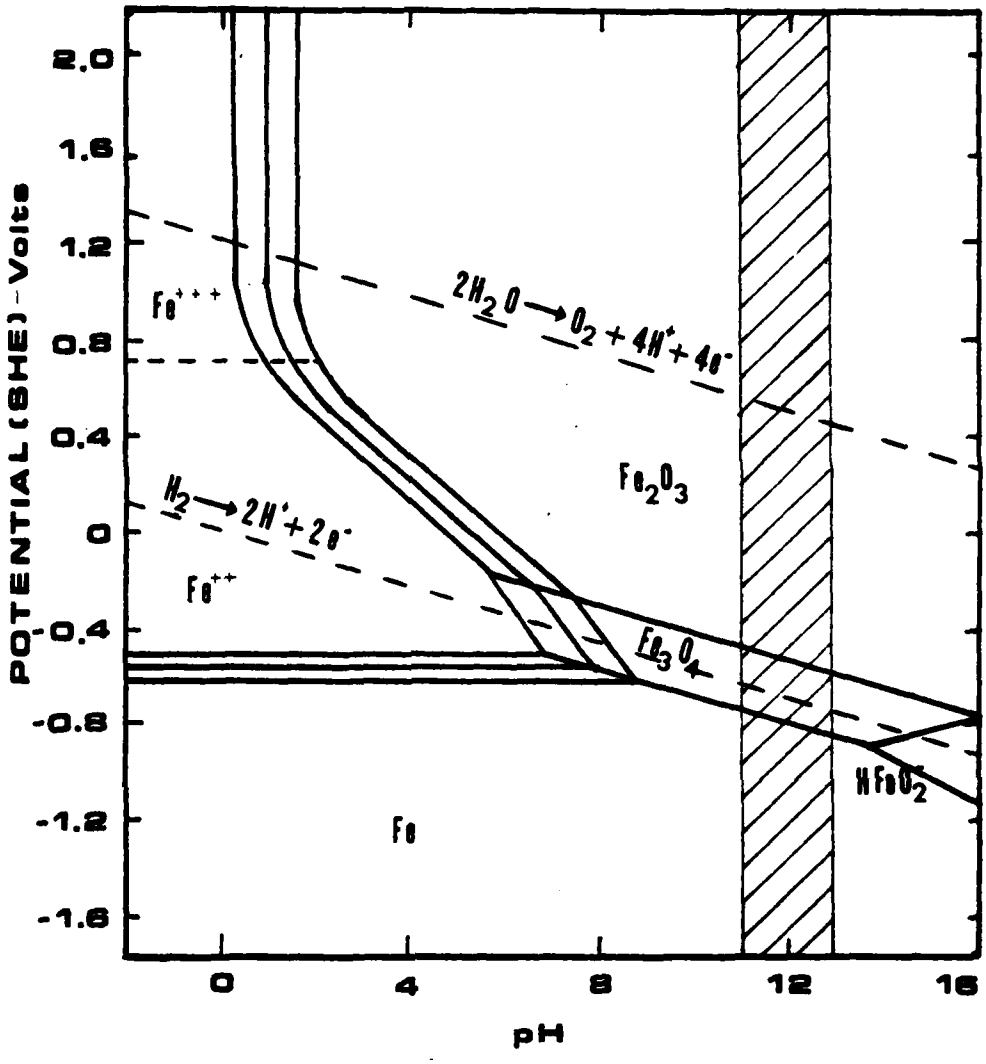

Figure E-1. Pourbaix Diagram for Iron

(Adapted from Atlas of Electrochemical Diagrams by Pourbaix)

expected values of pH for the environment in concrete. Lines (a) and (b) represent the oxidation-reduction reactions for oxygen and hydrogen respectively, at a pressure of 1.0 atm. By decreasing the O_2 pressure, the (a) line will be displaced in the negative direction. Conversely, decreasing the H_2 pressure will displace the (b) line in the positive direction. Applying polarization techniques, one notices that as the O_2 pressure is decreased or removed from the electrolyte, the potential difference between the O_2 redox line and the upper limit of the Fe immunity region is reduced. By applying Ohm's Law, $E = I/R$, where the resistance of the electrolyte remains unchanged, as the potential decreases, the current must also decrease thereby slowing the corrosion process.

TABLE E-II - Galvanic Series

Some Commercial Metals and Alloys in Seawater

↑ Noble or cathodic	Platinum
	Titanium
	Hastelloy C
	18/8 stainless steel (passive)
	Inconel 600 (passive)
	Monel
	Copper
Active or anodic	Steel or Iron
	Zinc
↓	Magnesium

II. PHYSICAL PROPERTIES OF 1020 STEEL AND OTHER REBAR MATERIALS

Tables E-III and E-IV give the properties of 1020 steel which was used as rebar material in this research.

TABLE E-III - Nominal Properties of 1020 Steel [45]

Nominal Composition	C %	MN %	P % (max)	S % (max)
	0.18 - 0.23	0.30 - 0.60	0.04	0.05

Property	Hot Rolled	Cold Rolled
Tensile Strength	55 ksi	61 ksi
Yield Strength	30 ksi	51 ksi
% Elongation in 2 in.	25 %	15 %
Reduction in Area	50 %	40 %
Hardness	71 R_B	76 R_B

The material is easily welded by all commercial processes.

TABLE E-IV - Measured Properties of 1020 Steel

Tensile Strength	61 ksi
Yield Strength	49 ksi
% Elongation in 1.5 in.	12 %
Reduction in Area	38 %
Hardness	77 R_B

Figures E-2 and E-3 show the ferritic-pearlitic microstructure of the 1020 steel used in this research.

Figure E-2. Optical Micrograph of Ferrite-Pearlite Structure of 1020 Steel. Magnification 400X.

Figure E-3. Optical Micrograph of Ferrite-Pearlite Structure of 1020 Steel. Magnification 2000X.

Concrete reinforcing bars are available in plain low carbon steels or in low alloy steels. The carbon content is generally 0.20 - 0.30%, and when low alloy steels are used the maximum carbon equivalent must not exceed 0.55, as calculated by the following formula:

$$CE = \%C + \%Mn/6 + \%Cu/40 + \%Ni/20 + \%Cr/10 - \%Mo/50 - \%V/10$$

Rebar is available as plain or deformed round bars. The deformed bars have raised lugs or protrusions, to improve bonding characteristics to the concrete, which are hot formed in the bar on the final pass between the rolling mills. Plain carbon rounds are usually adequate for most applications; but in applications where higher strength, ductility, weldability, or improved bending characteristics are desired, low alloy rounds may be used. Figure E-4 shows the different types of rebar that are commerically available.

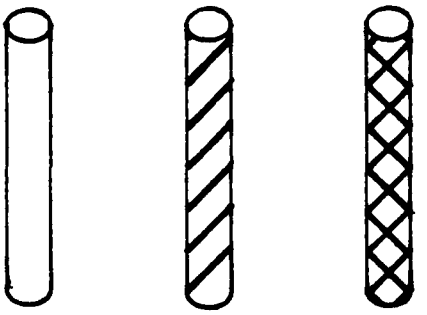

Figure E-4. Three common forms of rebar commercially available. (a) Straight rounds (b) Deformed rounds, spiral pattern (c) Deformed rounds, diamond pattern.

III. PHYSICAL PROPERTIES OF CONCRETE AND ITS CHEMICAL COMPOSITION [46]

Cement, when mixed with an aggregate and water, forms synthetic stone which is commonly referred to as concrete. The cement used in the formation of concrete is a mixture of compounds as shown by Figure E-5. The types of Portland Cement formed from these ingredients is shown in Figure E-6.

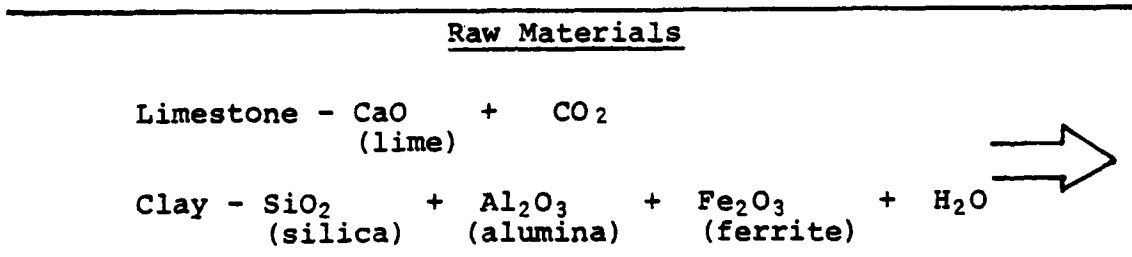

FIGURE E-5 - The Formation of Portland Cement

	Portland Cement Type				
	I	II	III	IV	V
C_3S	51	46	58	26	39
C_2S	25	32	16	54	43
C_3A	9	4	8	2	2
C_4AF	8	12	8	12	8
Others	7	6	10	6	8

FIGURE E-6 - Typical Proportions of Compounds Found in Portland Cement.

The addition of water to cement produces the following reactions:

$$2(3CaO \cdot SiO_2) + 6H_2O = 3CaO \cdot 2SiO_2 \cdot 3H_2O + 3Ca(OH)_2$$

$$2(2CaO \cdot SiO_2) + 4H_2O = 3CaO \cdot 2SiO_2 \cdot 3H_2O + Ca(OH)_2$$

$$4CaO \cdot Al_2O_3 \cdot Fe_2O_3 + 10H_2O + 2Ca(OH)_2 = 6CaO \cdot Al_2O_3 \cdot Fe_2O_3 \cdot 12H_2O$$

$$3CaO \cdot Al_2O_3 + 12H_2O + Ca(OH)_2 = 3CaO \cdot Al_2O_3 \cdot Ca(OH)_2 \cdot 12H_2O$$

$$3CaO \cdot Al_2O_3 + 10H_2O + CaSO_4 \cdot 2H_2O = 3CaO \cdot Al_2O_3 \cdot CaSO_4 \cdot 12H_2O$$

FIGURE E-7 - Hydration Reactions in Portland Cements

TABLE E-V - Typical Physical and

Mechanical Properties of Concrete

Property	Typical Values for Normal Concretes
Density	140 - 150 lb/ft^3
Porosity	5 - 10 %
Compressive Strength	3.5 - 5.5 ksi
Modulus of Elasticity	3.0×10^6 - 6.0×10^6 psi
Poisson's Ratio	0.16 - 0.26
Permeability	10^{-10} m/sec

LIST OF REFERENCES

1. Sharp, J.V., "Concrete Oil Production Platforms," The Metallurgist and Materials Technologist, pp. 13-16, 1981.

2. Kilareski, W.P., "Corrosion Induced Deterioration of Reinforced Concrete -- An Overview," Materials Performance Vol. 19 No. 3, pp. 48-50, March 1980.

3. Loc. cit.

4. Sharp, Loc. cit.

5. Sharp, Loc. cit.

6. Lewis, D.A., "Some Aspects of the Corrosion of Steel in Concrete," Metallic Corrosion, 1961, p. 548, Butterworths, 1962.

7. Bazant, Z.P., "Physical Model for Steel Corrosion in Concrete Sea Structures -- Theory," Journal of the Structural Division, ASCE, Vol. 105, No. 6, pp. 1137-1153, June 1979.

8. Kilareski, Loc. cit.

9. Lankard, D.R., "Cement and Concrete Technology for the Corrosion Engineer," Materials Performance, pp. 24-37, August 1976.

10. Whiting, D., Concrete Materials, Mix Design, Construction Practices and Their Effects on the Corrosion of Reinforcing Steel, paper presented at The International Corrosion Forum, Corrosion/78, Houston, TX, 6-10 March 1978.

11. Lankard, Loc. cit.

12. Cady, P.D., "Corrosion of Reinforcing Steel, in Significance of Tests and Properties of Concrete and Concrete-Making Materials," Special Technical Publication, STP 169B, American Society for Testing and Materials, pp. 275-299, December 1978.

13. Mehta, P.K., "Effect of Cement Composition of Corrosion of Reinforcing Steel in Concrete," Chloride Corrosion of Steel in Concrete, STP-629, edited by D.E. Tonini and S.W. Dean, Jr., American Society for testing and Materials, pp. 12-19, 1977.

14. Robinson, R.C., "Design of Reinforced Concrete Structures for Corrosive Environments," Materials Performance, Vol. 11, No. 3, pp. 15-19, March 1972.

15. Dawson, J.L., and others, Electrochemical Impedance Measurements Applied to the Corrosion of Reinforcing Steel in Concrete, paper presented at The International Corrosion Forum, Corrosion/78, Houston, TX, 6-10 March 1978.

16. Dehghanian, C., and Locke, C.E., Imbeddable Reference Electrodes for Chloride Contaminated Concrete, paper presented at The International Corrosion Forum, Corrosion/78, Houston, TX, 6-10 March 1978.

17. Keldsen, T.J., Measuring Steel-in-Concrete Corrosion with an Electrical Resistance Probe, paper presented at The International Corrosion Forum, Corrosion/78, Houston, TX, 6-10 march 1978.

18. Deskins, R.L., Cathodic Protection Requirements for Concrete Pipes, paper presented at The International Corrosion Forum, Corrosion/78, Houston, TX, 6-10 March 1978.

19. Cady, Loc. cit.

20. Vrable, J.B. and Wilde, B.E., "Electrical Potential Requirements for Cathodic Protection of Steel in Simulated Concrete Environments," Corrosion, Vol. 36, No. 1, pp. 18-23, January 1980.

21. Whiting, Loc. cit.

22. Cady, Loc. cit.

23. Gaidas, J.M. and Rosenberg, A.M., The Mechanism of Nitrite Inhibition of Chloride Attack on Reinforcing Steel in Alkaline Aqueous Environments, paper presented at the International Corrosion Forum, Corrosion/78, 6-10 March 1978.

24. Gaidas, J.M., Lundquist, J.T., Jr., and Rosenberg, A.M., "Calcium Nitrite as an Inhibitor of Rebar Corrosion in Chloride Containing Concrete," Materials Performance, Vol. 18, No. 3, pp. 36-40, March 1979.

25. Abdul Azim, A.A., Gouda, V.K., and El-Sayed, H.A., "The Effect of Stress on the Corrosion Behavior of Mild Steel in Alkaline Solutions," Corrosion Science, Vol. 9, pp. 215-224, 1979.

26. Robinson, Loc. cit.

27. Deskins, Loc. cit.

28. Cook, A.R. and Tonini, D.E., The Performance of Galvanized Reinforcement in High Chloride Environments -- Field Study Results, paper presented at The International Corrosion Forum, Corrosion/78, Houston, TX, 6-10 March 1978.

29. Kilareski, W.P., "Epoxy Coatings for Corrosion Protection of Reinforcement Steel," Chloride Corrosion of Steel in Concrete, STP-629, edited by D.E. Tonini and S.W. Dean, Jr., American Society for Testing and Materials, pp. 82-88, 1977.

30. Slater, J.E., Corrosion of Reinforcing Steel in Concrete: Magnitude of the Problem, paper presented at The International Corrosion Forum, Corrosion/78, Houston, TX, 6-10 March 1978.

31. Kuckacka, L.E., "The Use of Concrete Polymer Materials for Bridge Deck Applications," Chloride Corrosion of Steel in Concrete, STP-629, edited by D.E. Tonini and S.W. Dean, Jr., American Society for Testing and Materials, pp. 110-115, 1977.

32. Abdul Azim, Loc. cit.

33. Haussmann, D.A., "Steel Corrosion in Concrete -- How Does it Occur?" Materials Protection, pp. 19-23, November 1967.

34. Gjørv, O.E. and Vennesland, Ø., "Diffusion of Chloride Ions from Seawater into Concrete," Cement and Concrete Research, Vol. 9, No. 2, pp. 229-238, March 1978.

35. Monfore, G.E. and Ost, Borje, "Penetration of Chloride into Concrete," Journal of the Portland Cement Association Research and Development Laboratories, 8(11), pp. 46-52, January 1966.

36. El-Busaidy, A.H.S., Gjørv, O.E., and Vennesland, Ø., Diffusion of Dissolved Oxygen Through Concrete, paper presented at The International Corrosion Forum, Corrosion/76, Houston, TX, 22-26 March 1976.

37. Ailor, W.H., Handbook on Corrosion Testing and Evaluation, pp. 181-183, Wiley, 1971.

38. Verbeck, G.J., "Mechanisms of Corrosion of Steel in Concrete," ACI SP-49, Corrosion of Metals in Concrete, pp. 21-38, 1975.

39. Ibid., p. 25.

40. Bazant, Loc. cit.

41. Abdul Azim, Loc. cit.

42. Haussmann, Loc. cit.

43. Bazant, Loc. cit.

44. Latimer, W.M., Oxidation Potentials, Second ed., Prentice-Hall, pp. 345-348, 1952.

45. Parker, E.R., Materials Data Book, McGraw-Hill, pp. 6-7, 1967.

46. Lankard, Loc. cit.

BIBLIOGRAPHY

Annual ASTM Standards, 1975 ed., part 10, pp. 626-696, American Society for Testing and Materials, 1975.

Argonne National Laboratory Report ANL/OTEC-BCM-010, Antifouling Marine Concrete, by H.P. Vind and C.W. mathews, July 1980.

Atkins, P.O., Physical Chemistry, Oxford University Press, 1978.

Azevedo, W.V., Deen, R.C., Havens, J.H. and Rahal, A.S., "Cracking in Concrete Pavements," Transportation Engineering Journal, ASCE, Vol. 10, No. TE2, March 1980.

Balasubramanian, T.M., Rajagopalan, K.S. and Rengaswany, N.S., "Some Aspects of Reinforcement Corrosion and Its Prevention: Work Carried Out at the Central Electrochemical Research Institute, Karaikudi," Journal of Scientific and Industrial Research (New Delhi, India), Vol. 28, No. 10, 1969.

Bazant, Z.P., "Physical Model for Steel Corrosion in Concrete Sea Structures -- Applications," Journal of the Structural Division, ASCE, Vol. 105, No. 6, June 1979.

Cummings, J.R., Galvanic Aspects of Aluminum Sacrificial Anode Alloys in Seawater, M.S. Thesis, Naval Postgraduate School, Monterey, California, December 1977.

Fontanna, M.G.and Greene, N.D., Corrosion Engineering, McGraw-Hill, 1967.

Graham, K.J., Microgalvanic Aspects of the Seawater Corrosion of Marine Materials in the Presence of Hypochlorite Ion Fouling Inhibitor, M.S. Thesis, Naval Postgraduate School, Monterey, California, December 1979.

Handbook of Chemistry and Physics, 60th ed., CRC Press, 1979.

Leumer, G.H., Effects of Hydrodynamic Variables on Corrosion: Study of 90/10 Cu-Ni In a Circling Foil with Synthetic Seawater, M.S. Thesis, Naval Postgraduate School, Monterey, California, March 1979.

Metals Handbook, 8th ed., v. 1,2,7, American Society for Metals, 1964.

Neville, A.M., Hardened Concrete: Physical and Mechanical Aspects, American Concrete Institute and the Iowa State University Press, 1971.

Page, C.L., "Mechanism of Corrosion Protection in Reinforced Concrete Marine Structures," Nature, Vol. 258, December 1975.

Pourbaix, M., Lectures on Electrochemical Corrosion, Plenum Press, 1973.

Roberts, J.L. and Sawyer, D.T., Experimental Electrochemistry for Chemists, Wiley, 1974.

Shreir, L.L., Corrosion, 2nd ed., v. 1,2, Newnes-Butterworths, 1977.

Spellman, D.L. and Stratfull, R.F., "Concrete Variables and Corrosion Testing," Highway Research Record, No. 423, 1973.

Tomashov, N.D., Theory of Corrosion and Protection of Metals, Macmillan, 1966.

Uhlig, H.H., Corrosion and Corrosion Control, Second ed., Wiley, 1971.

Uhlig, H.H., The Corrosion Handbook, Wiley, 1948.

Whitehurst, E.H., Evaluation of Concrete Properties from Sonic Tests, American Concrete Institute and the Iowa State University Press, 1966.

Wilkins, N., "International Seminar: Electrochemistry and Corrosion of Steel-in-Concrete -- A State-of-the-Art Summary," Materials Performance, Vol. 19, No. 5, 1980.

INITIAL DISTRIBUTION LIST

		No. Copies
1.	Defense Technical Information Center Cameron Station Alexandria, Virginia 22314	2
2.	Library, Code 0142 Naval Postgraduate School Monterey, California 93940	2
3.	Department Chairman, Code 69Mx Department of Mechanical Engineering Naval Postgraduate School Monterey, California 93940	1
4.	Professor A. J. Perkins, Code 69Ps Department of Mechanical Engineering Naval Postgraduate School Monterey, California 93940	2
5.	Professor R. A. Reinhardt, Code 61Ri Department of Physics and Chemistry Naval Postgraduate School Monterey, California 93940	1
6.	Dr. R. W. Drisko Materials Science Division Civil Engineering Laboratory Port Hueneme, California 93043	1
7.	LT Dale R. Scott, USN 3159 Fairbury Lane Fairfax, Virginia 22030	2
8.	Mr. James Jenkins Materials Science Division Civil Engineering Laboratory Port Hueneme, California 93043	1
9.	Mr. Dan Pauley Materials Science Division Civil Engineering Laboratory Port Hueneme, California 93043	1

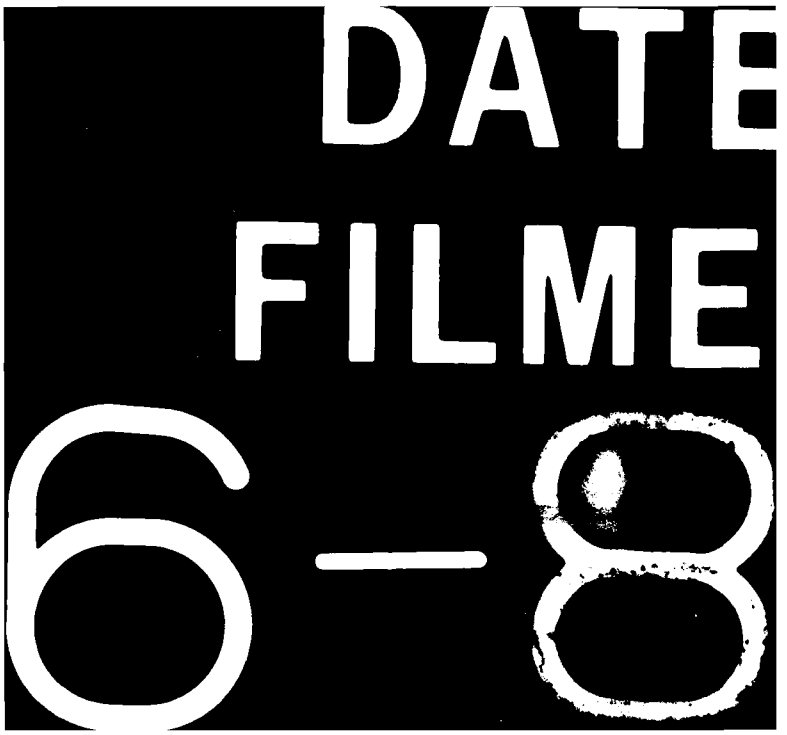
DATE
FILME
6-8